Boundary Matching Filters for Spherical Microphone and Loudspeaker Arrays

César D. Salvador, Shuichi Sakamoto, Jorge Treviño, and Yôiti Suzuki *Member, IEEE*

Abstract—Conversion of microphone array signals into loudspeaker array signals is an essential process in high-definition spatial audio. This paper presents the theory of boundary matching filters (BMFs) for spherical array signal conversion. BMFs adapt the physical boundary conditions used during recording to the ones required for reproduction by relying on a theoretical framework provided by the Kirchhoff–Helmholtz integral equation (KHIE). Computationally, array signal conversion is performed in a transform domain where sound fields are represented in terms of spherical harmonic functions. Related research on transform-domain signal conversion filters is interpreted in the context of the KHIE. The case of a rigid recording boundary and an open reproduction boundary is addressed. The proposed rigid-to-open BMFs provide a suitable basis for designing gain-limited filters to deal with the problem of excessive gains at certain frequency bands, observed when using high-resolution arrays. Spatial, spectral, and temporal effects in sound field reconstruction when finite numbers of transducers are used in anechoic conditions are investigated analytically and exemplified numerically. Results show that the proposed gain-limited rigid-to-open BMFs outperform the existing gain-limited filters based on Tikhonov regularization because they reduce the spatial discretization effects and yield impulse responses that are more localized around their main peaks.

Index Terms—Spatial audio, sound field recording, sound field reproduction, Kirchhoff–Helmholtz integral equation, array signal processing, spherical array, spherical Fourier transform.

I. INTRODUCTION

CONVERSION of microphone array pressure signals into loudspeaker array driving signals is an essential process in high-definition spatial audio. Array signal conversion involves the adaptation of the physical boundary conditions used during recording to the ones required for reproduction. Unifying theories for physically motivated spatial audio [1]–[3] suggest obtaining signal conversion filters by linking the examinations of the Kirchhoff–Helmholtz integral equation (KHIE) [4] on the recording and reproduction boundaries. Such filters are referred to in this paper as boundary matching filters (BMFs).

Spherical boundaries are useful because they provide symmetry and emphasize the central listening region. They also

C. D. Salvador, S. Sakamoto, J. Treviño, and Y. Suzuki are with the Research Institute of Electrical Communication (RIEC) and the Graduate School of Information Sciences (GSIS), Tohoku University, Sendai 980-8577, Japan (e-mail: salvador@ais.riec.tohoku.ac.jp, saka@ais.riec.tohoku.ac.jp, jorge@ais.riec.tohoku.ac.jp, and yoh@riec.tohoku.ac.jp).

enable the analytical formulation of spherical BMFs (SBMFs) in a transform domain where sound fields are represented in terms of spherical harmonic functions of distinct orders [4]. These functions are orthonormal on the unit sphere and define the spherical Fourier transform (SFT) and the inverse spherical Fourier transform (ISFT) [5]. Implementations with spherical arrays facilitate the transform-domain processing at scalable angular resolutions parameterized by orders of the SFT. The design of SBMFs for high-resolution arrays, however, still represents a challenge for the realization of high-definition spatial audio systems.

In recording, a rigid baffle supporting the array is used as an acoustically rigid boundary to allow for resonance-free sound field representations from measurements of only pressure [1]. The KHIE under the Neumann boundary condition [4] models this case for the subsequent inversion of the rigid sphere model, a necessary step for obtaining free-field representations. In reproduction, whether using real or virtual loudspeakers, a simplification of the KHIE known as the principle of acoustic wave superposition [6] is used to enable sound field reconstruction from monopole-like loudspeakers [7]. Loudspeakers radiating plane waves are equivalent to the consideration of a boundary of infinite size (far field), whereas the case of spherical waves is equivalent to a boundary of finite size (near field).

SBMFs under the above conditions are equivalent to the transform-domain inversion filters used in microphone array studies, including sound field encoding [8], [9], beamforming [10]–[21], binaural synthesis [22]–[32], and room acoustics [33]–[36]. A well-known difficulty is the ill-posedness of the inversion problem that produces filters with excessive gains in certain frequency bands at higher orders. A less explored aspect is the reproduction boundary condition that underlies these filters. Although monopole-like loudspeakers are implicitly assumed in free field, acoustic superposition is also apparently equivalent to reconstruction with loudspeakers placed on the inner surface of an acoustically rigid spherical cavity [7], which may be impractical because of the resonances that occur within [37]. The reproduction boundary condition remains ambiguous when relying simply on acoustic superposition. To overcome this ambiguity, it would be useful to examine the case of having an acoustically transparent or open boundary for reproduction in the light of the KHIE.

Excessive gains are inherent to high-order SFT representations. Gain-limitation methods for high-resolution arrays have been partially covered in studies of microphone arrays [10]–[12], [14]–[21], loudspeaker arrays [38]–[41], and their combined use [13], [42]–[45]. General-purpose meth-

ods include frequency-dependent order truncation [46] and Tikhonov regularization [9], [18], [30]–[32]. Other methods include spherical-cap windowing [47], gain thresholding [18], [48], low-to-high order equalization [49], [50], and filter banks [19]. Limitation of gain by considering the boundary conditions in the context of the KHIE, however, has not been addressed in previous studies. The spatial, spectral, and temporal effects of gain limitation are also issues requiring further attention.

This paper derives SBMFs for a rigid recording boundary and an open reproduction boundary. Reproduction is modeled with an alternative version of the KHIE known as the simple source formulation [51]. A continuity condition is further chosen to link recording and reproduction. The resulting SBMFs smoothly assign high-order components to high-frequency bands in agreement with the far-to-near field transitions. As an alternative to existing gain-limited SBMFs, the proposed SBMFs further provide a suitable basis for designing smooth and bounded SBMFs for high-resolution arrays by the assignment of smaller listening areas to higher frequencies while the order truncation error is kept bounded.

The remainder of this paper is organized as follows. Section II provides a theoretical framework and overviews the existing rigid-to-infinite (RI) and rigid-to-finite (RF) SBMFs that rely on reproduction by acoustic superposition. Section III presents the proposed rigid-to-open (RO) SBMFs that rely on reproduction by simple source formulation. Section IV describes two existing general-purpose gain-limitation methods (sections IV-A and IV-B) and presents a new gain-limitation method for RO-SBMFs (section IV-C); the effects of gain limitation are investigated in the context of angular bandwidth limitation. Section V investigates the effects of sampling based on analyses of orthonormality errors. Concluding remarks are given in section VI.

II. RIGID-TO-INFINITE AND RIGID-TO-FINITE SBMFs

Transform-domain filters for array signal conversion are overviewed in this section. They are interpreted here as SBMFs obtained by examining the KHIE in both the recording and the reproduction boundaries. The KHIE is detailed in appendix A.

A. Continuous-space geometry and physical considerations

Figures 1 and 2 detail the spherical geometries used in this paper. In recording, the KHIE under the Neumann boundary condition [4], on rigid boundary $\mathcal{A}$, is used to obtain the pressure field in free field at $\vec{b}$. In reproduction, a simplified version of the KHIE, known as the principle of acoustic wave superposition [6], on boundary $\mathcal{B}$, is used to reconstruct the sound field at arbitrary $\vec{r}$.

All of what follows considers acoustic waves satisfying the Helmholtz equation with time-harmonic dependence $\exp(-jkct)$, where k denotes the wave number, c is the speed of sound in air, and $j = \sqrt{-1}$ is the "positive" imaginary unit. The radial part of the diverging waves emanating outward from a source is modeled by the spherical Hankel function of the first kind and order ν, denoted here by h_ν^{out}. The radial part of the converging waves coalescing inward to a sink is modeled
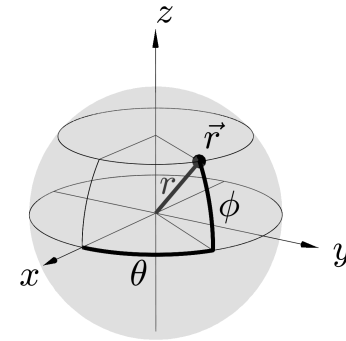

Fig. 1. Spherical coordinate system. A point in space $\vec{r} = (r, \theta, \phi)$ is specified by its radial distance r, azimuth angle $\theta \in [-\pi, \pi]$, and elevation angle $\phi \in [-\frac{\pi}{2}, \frac{\pi}{2}]$. Angles are merged into the variable $\Omega = (\theta, \phi)$ in such a way that a point in space is also represented by $\vec{r} = (r, \Omega)$.

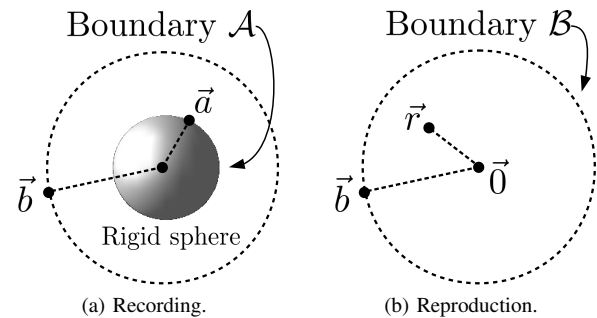
(a) Recording.   (b) Reproduction.

Fig. 2. Recording and reproduction boundaries. The recording boundary $\mathcal{A}$ is composed of recording points $\vec{a} = (a, \Omega_a)$. The reproduction boundary $\mathcal{B}$ is composed of secondary source points $\vec{b} = (b, \Omega_b)$. The sizes of $\mathcal{A}$ and $\mathcal{B}$ are such that $0 < a < b$. The boundary $\mathcal{B}$ divides the space into an exterior and an interior volume. The point $\vec{r}$ in the interior volume denotes an arbitrary position at which the sound pressure is reconstructed. The centers of $\mathcal{A}$ and $\mathcal{B}$ are both in the origin $\vec{0}$ of the coordinate system in Fig. 1.

by the spherical Hankel function of the second kind and order ν, denoted here by h_ν^{in}. The derivative of any h_ν with respect to its argument is denoted by h_ν'. The angular part of the waves is modeled by the spherical harmonic functions of order ν and degree μ, denoted here by Y_ν^μ and defined by (52) in appendix B. These angular functions conform an orthonormal basis that enables the spherical Fourier transform (SFT) and the inverse spherical Fourier transform (ISFT), respectively defined by (55) and (54) in appendix B. The SFT and ISFT isomorphically relate the representations of a function in the spatial domain (the unit sphere) and the transform domain (ν and μ). All waves under consideration satisfy the Sommerfeld radiation condition at infinity, and all analyses are restricted to anechoic conditions.

B. General framework

The unified recording and reproduction framework for the reconstruction of pressure is summarized in Fig. 3. In the spatial domain, the acoustic pressure Ψ at arbitrary point $\vec{r}$ is modeled by acoustic wave superposition [6] as follows:

$$\Psi(\vec{r}, k) = \int_{\Omega_b \in \mathcal{B}} \mathcal{T}(\vec{b}, \vec{r}, k) \mathcal{D}(\vec{b}, k) d\Omega_b, \qquad (1)$$

where $\mathcal{D}$ is a distribution of pressure on $\mathcal{B}$, and $\mathcal{T}$ is an acoustic transfer function modeling sound transmission from $\vec{b}$ to $\vec{r}$.

(a) Combination of $\mathcal{D}$ and $\mathcal{T}$ in spatial domain.

(b) Combination of $\mathcal{D}$ and $\mathcal{T}$ in transform domain.
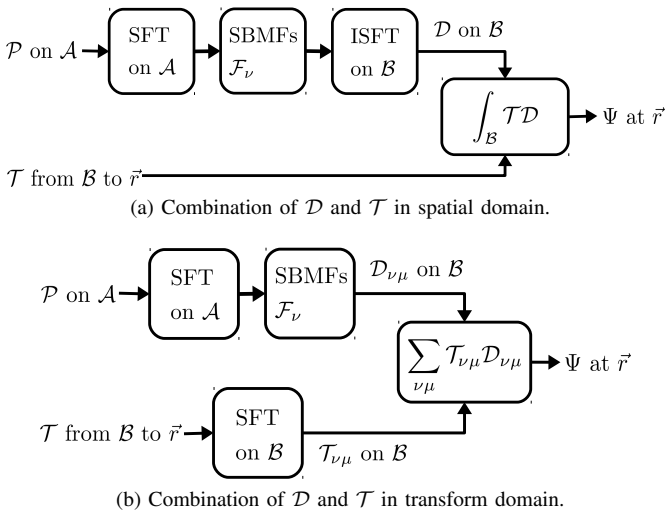
Fig. 3. Reconstruction of pressure Ψ at arbitrary $\vec{r}$ from pressure recordings $\mathcal{P}$ on $\mathcal{A}$ and acoustic transfer functions $\mathcal{T}$ from $\mathcal{B}$ to $\vec{r}$. SBMFs convert $\mathcal{P}$ on $\mathcal{A}$ into driving signals $\mathcal{D}$ on $\mathcal{B}$. Combination of $\mathcal{D}$ and $\mathcal{T}$ is equivalently performed in the spatial (a) or transform (b) domain. Representations in the spatial and transform domains are isomorphically related via the spherical Fourier transform (SFT) and the inverse spherical Fourier transform (ISFT).

Depending on the targeted application, $\mathcal{D}$ can represent driving signals for an array of real or virtual loudspeakers on $\mathcal{B}$, whereas $\mathcal{T}$ can represent free-field transfer functions, room transfer functions, or head-related transfer functions.

Owing to orthonormality in (53), reconstruction based on (1) is equivalently formulated in the transform domain as follows:

$$\Psi(\vec{r}, k) = \sum_{\nu=0}^{\infty} \sum_{\mu=-\nu}^{\nu} \mathcal{T}_{\nu\mu}(b, \vec{r}, k) \mathcal{D}_{\nu\mu}(b, k), \qquad (2)$$

where $\mathcal{T}_{\nu\mu}$ denotes the SFT of $\mathcal{T}$ over $\mathcal{B}$, explicitly

$$\mathcal{T}_{\nu\mu}(b, \vec{r}, k) = \int_{\Omega_b \in \mathcal{B}} \mathcal{T}(\vec{b}, \vec{r}, k) \overline{Y_\nu^\mu(\Omega_b)} d\Omega_b, \qquad (3)$$

and $\mathcal{D}_{\nu\mu}$ denotes the SFT of $\mathcal{D}$ over $\mathcal{B}$. The overbar denotes complex conjugate.

SBMFs aim to calculate $\mathcal{D}$ on $\mathcal{B}$ from $\mathcal{P}$ on $\mathcal{A}$ based on

$$\mathcal{D}_{\nu\mu}(b, k) = \mathcal{F}_\nu(a, b, k) \mathcal{P}_{\nu\mu}(a, k), \qquad (4)$$

where $\mathcal{F}_\nu$ are transform-domain SBMFs for concentric spherical boundaries $\mathcal{A}$ and $\mathcal{B}$, and $\mathcal{P}_{\nu\mu}$ is the SFT of $\mathcal{P}$ over $\mathcal{A}$:

$$\mathcal{P}_{\nu\mu}(a, k) = \int_{\Omega_a \in \mathcal{A}} \mathcal{P}(\vec{a}, k) \overline{Y_\nu^\mu(\Omega_a)} d\Omega_a. \qquad (5)$$

When required, $\mathcal{D}$ can be obtained by ISFT as

$$\mathcal{D}(\vec{b}, k) = \sum_{\nu=0}^{\infty} \sum_{\mu=-\nu}^{\nu} \mathcal{D}_{\nu\mu}(b, k) Y_\nu^\mu(\Omega_b). \qquad (6)$$

C. Transform-domain SBMFs

A reproduction boundary composed of secondary sources radiating plane waves is equivalent to a boundary $\mathcal{B}$ of infinite radius. Correspondingly, SBMFs are formulated by transform-domain inversion of the model for acoustic scattering from the rigid boundary $\mathcal{A}$ due to an incident plane wave:

$$\mathcal{F}_\nu^{\text{RI}}(a, k) = \frac{(ka)^2 h_\nu'^{\text{out}}(ka)}{4\pi j^{\nu+1}}, \quad \text{Rigid } \mathcal{A} \text{ Infinite } \mathcal{B}. \qquad (7)$$

On the other hand, a reproduction boundary that consists of secondary sources radiating spherical waves is equivalent to a boundary $\mathcal{B}$ of finite radius. In this case, SBMFs are formulated by transform-domain inversion of the model of acoustic scattering from the rigid boundary $\mathcal{A}$ due to an incident spherical wave:

$$\mathcal{F}_\nu^{\text{RF}}(a, b, k) = \frac{-ka^2 h_\nu'^{\text{out}}(ka)}{4\pi h_\nu^{\text{out}}(kb)}, \quad \text{Rigid } \mathcal{A} \text{ Finite } \mathcal{B}. \qquad (8)$$

SBMFs in (7) and (8) remove the scattering of the rigid spherical baffle. SBMFs in (8) further extrapolate along distance (from $\mathcal{A}$ to $\mathcal{B}$) the resulting free-field representation. Both SBMFs are recognized in the literature as terms inversely proportional to the SFT of the Green-Neumann function [4], or inversely proportional to the singular values of the rigid sphere model [32], [52]. They are also identified as the reciprocal of the source mode strengths [10]–[15], [17], [20], [22]–[26], [33]–[36], [44], [45], [53] or included in what is commonly referred to as a radial filter [8], [9], [16], [18], [19], [30]–[32]. Special attention is given hereafter to the SBMFs in (8) because of their importance in near-field applications.

D. Interpretation in the context of the KHIE

The link between recording and reproduction in (4) is clarified here by separate examinations of the KHIE in (51) on the spherical bounding surfaces $\mathcal{A}$ and $\mathcal{B}$, where the normal derivative $\frac{\partial}{\partial \vec{n}_s}$ in (51) is reduced to the radial derivative $\frac{\partial}{\partial r}$.

In recording, the KHIE is used to obtain the sound pressure in free-field at observation point $\vec{b}$ from its values on $\mathcal{A}$ under the Neumann boundary condition. The source-free volume containing $\vec{b}$ is taken outside $\mathcal{A}$ except in some vicinities containing the sound sources. At infinity, the Sommerfeld radiation condition is assumed. Considering first a generic observation point $\vec{r}$, such that $r \geq a$, recording is modeled as the following exterior problem:

$$\mathcal{P}^{\text{ff}}(\vec{r}) = - \int_{\Omega_a \in \mathcal{A}}$$
$$\left[\mathcal{T}^{\mathcal{N}}(\vec{a}, \vec{r}) \frac{\partial}{\partial r} \mathcal{P}^{\text{ff}}(\vec{r}) \Big|_{r=a} - \mathcal{P}^{\text{ff}}(\vec{a}) \frac{\partial}{\partial r} \mathcal{T}^{\mathcal{N}}(\vec{a}, \vec{r}) \right] d\Omega_a. \qquad (9)$$

Here, $\mathcal{P}^{\text{ff}}$ denotes free-field pressure, and $\mathcal{T}^{\mathcal{N}}$ denotes the Green-Neumann function. This function fulfills the Neumann boundary condition, $\frac{\partial}{\partial r} \mathcal{T}^{\mathcal{N}}(\vec{a}, \vec{r}) = 0$, and its SFT over $\mathcal{A}$ is $\mathcal{T}_{\nu\mu}^{\mathcal{N}} \propto \overline{1/\mathcal{F}_\nu}$ [4]. The generic point is set to $\vec{r} = \vec{b}$, such that $b > a$. By writing the integrands of (9) in terms of their ISFTs, and using acoustic reciprocity to exchange $\vec{a}$ and $\vec{b}$, it has been shown in [4], [52] that

$$\partial \mathcal{P}_{\nu\mu}^{\text{ff}}(b, k) = \mathcal{F}_\nu^{\text{RF}}(a, b, k) \mathcal{P}_{\nu\mu}(a, k), \qquad (10)$$

where $\partial \mathcal{P}_{\nu\mu}^{\text{ff}}$ denotes the SFT of $\frac{\partial}{\partial r} \mathcal{P}^{\text{ff}}$ on $\mathcal{B}$, and $\mathcal{P}_{\nu\mu}$ indicates pressure on $\mathcal{A}$ before scattering removal and radial extrapolation.

In reproduction, acoustic wave superposition in (1) is apparently equivalent to using the KHIE for reconstructing the sound pressure at arbitrary observation point $\vec{r}$ from its values on $\mathcal{B}$. Assuming that scattering was removed during recording, the source-free volume containing $\vec{r}$ is now taken inside $\mathcal{B}$,

that is, $r \leq b$. This case would constitute an interior problem formulated as

$$\Psi(\vec{r}) = \mathcal{D}(\vec{r}) = \int_{\Omega_b \in \mathcal{B}} \left[\mathcal{T}(\vec{b}, \vec{r}) \frac{\partial}{\partial r} \mathcal{D}(\vec{r}) \Big|_{r=b} - \mathcal{D}(\vec{b}) \frac{\partial}{\partial r} \mathcal{T}(\vec{b}, \vec{r}) \right] d\Omega_b, \tag{11}$$

under the assumption $\frac{\partial}{\partial r} \mathcal{T}(\vec{b}, \vec{r}) = 0$. When the integrands of (11) are expressed in terms of their ISFTs, it can be verified that the choice

$$\mathcal{D}_{\nu\mu}(b, k) = \partial \mathcal{P}_{\nu\mu}^{\text{ff}}(b, k) \tag{12}$$

would thus yield (4). A similar premise is used in the theory of wave field synthesis [7] to overcome the necessity of using dipole secondary sources, thereby enabling reproduction by using only monopole-like loudspeakers. The KHIE with vanishing radial derivatives on $\mathcal{B}$, however, proves to be the case of using loudspeakers placed on the inner surface of an acoustically rigid spherical cavity that would produce SBMFs affected also by the resonances inside cavities [37].

SBMFs in (8) certainly do not correspond to the condition that uses a rigid cavity for reproduction. Nevertheless, when modeling reproduction based on acoustic wave superposition, if one radial derivative in the KHIE is simply discarded without modifying the transfer functions, the physical conditions used during reproduction remain ambiguous. To overcome this ambiguity, the case of using an open boundary for reproduction is addressed in the next section by relying on an alternative version of the KHIE referred to as the simple source formulation [51].

III. RIGID-TO-OPEN SBMFs

This section derives the proposed SBMFs that convert $\mathcal{P}$ on rigid $\mathcal{A}$ into $\mathcal{D}$ on open $\mathcal{B}$. Open $\mathcal{B}$ is modeled by separately posing an interior problem and an exterior problem based on the simple source formulation [51] of the KHIE and by imposing a continuity condition on $\mathcal{B}$. The aim is to show that reproduction with open $\mathcal{B}$ is equivalent to modifying (12) according to the following expression:

$$\mathcal{D}_{\nu\mu}(b, k) = \mathcal{O}_\nu(b, k) \times \partial \mathcal{P}_{\nu\mu}^{\text{ff}}(b, k), \tag{13}$$

where $\mathcal{O}_\nu$ are the transform-domain open boundary filters

$$\mathcal{O}_\nu(b, k) = \left| \frac{j}{(kb)^2 h_\nu^{\text{in}}(kb) h_\nu^{\prime\text{out}}(kb)} \right|. \tag{14}$$

A new set of SBMFs relating a rigid $\mathcal{A}$ and an open $\mathcal{B}$ can thus be defined by equating (13) and (10), which yields

$$\mathcal{F}_\nu^{\text{RO}}(a, b, k) = \mathcal{O}_\nu(b, k) \times \mathcal{F}_\nu^{\text{RF}}(a, b, k), \text{ Rigid } \mathcal{A} \text{ Open } \mathcal{B}. \tag{15}$$

The formulation of (13), (14), and (15) is detailed hereafter. The integral in (1) is first interpreted in terms of the simple source formulation of the KHIE [51]. In this context, $\mathcal{T}$ is the free-field Green function, and $\mathcal{D}$ is the density distribution of simple sources or monopoles calculated from the radial derivatives of the sound field radiated inside and outside [51]:

$$\mathcal{D}(\vec{b}, k) = \frac{\partial}{\partial r} \Psi^{\text{int}}(\vec{b}, k) - \frac{\partial}{\partial r} \Psi^{\text{ext}}(\vec{b}, k). \tag{16}$$

Here, superscripts "int" and "ext" indicate that radial derivatives on $\mathcal{B}$ are calculated by pointing toward the interior and exterior volumes, respectively. The SFT of (16) results in

$$\mathcal{D}_{\nu\mu}(b, k) = \partial \Psi_{\nu\mu}^{\text{int}}(b, k) - \partial \Psi_{\nu\mu}^{\text{ext}}(b, k), \tag{17}$$

where $\partial \Psi_{\nu\mu}^{\text{int}}$ and $\partial \Psi_{\nu\mu}^{\text{ext}}$ are the SFTs of $\frac{\partial}{\partial r} \Psi^{\text{int}}$ and of $\frac{\partial}{\partial r} \Psi^{\text{ext}}$, respectively.

Let pressure fields in the vicinity of $\mathcal{B}$ be denoted by

$$\Psi^{\text{int}}(\vec{r}, k) = \sum_{\nu=0}^{\infty} \sum_{\mu=-\nu}^{\nu} \underbrace{\alpha_{\nu\mu}^{\text{in}}(k) h_\nu^{\text{in}}(kr)}_{\Psi_{\nu\mu}^{\text{int}}(r,k)} Y_\nu^\mu(\Omega),$$

$$\Psi^{\text{ext}}(\vec{r}, k) = \sum_{\nu=0}^{\infty} \sum_{\mu=-\nu}^{\nu} \underbrace{\alpha_{\nu\mu}^{\text{out}}(k) h_\nu^{\text{out}}(kr)}_{\Psi_{\nu\mu}^{\text{ext}}(r,k)} Y_\nu^\mu(\Omega), \tag{18}$$

where $\alpha_{\nu\mu}^{\text{in}}$ and $\alpha_{\nu\mu}^{\text{out}}$ are mode strengths. Their corresponding radial derivatives result in

$$\frac{\partial}{\partial r} \Psi^{\text{int}}(\vec{r}, k) = \sum_{\nu=0}^{\infty} \sum_{\mu=-\nu}^{\nu} \underbrace{\alpha_{\nu\mu}^{\text{in}}(k) k h_\nu^{\prime\text{in}}(kr)}_{\partial \Psi_{\nu\mu}^{\text{int}}(r,k)} Y_\nu^\mu(\Omega),$$

$$\frac{\partial}{\partial r} \Psi^{\text{ext}}(\vec{r}, k) = \sum_{\nu=0}^{\infty} \sum_{\mu=-\nu}^{\nu} \underbrace{\alpha_{\nu\mu}^{\text{out}}(k) k h_\nu^{\prime\text{out}}(kr)}_{\partial \Psi_{\nu\mu}^{\text{ext}}(r,k)} Y_\nu^\mu(\Omega). \tag{19}$$

Invariance of $\alpha_{\nu\mu}^{\text{in}}$ and $\alpha_{\nu\mu}^{\text{out}}$ along r leads to

$$\partial \Psi_{\nu\mu}^{\text{int}}(r, k) = \frac{k h_\nu^{\prime\text{in}}(kr)}{h_\nu^{\text{in}}(kr)} \Psi_{\nu\mu}^{\text{int}}(r, k),$$

$$\partial \Psi_{\nu\mu}^{\text{ext}}(r, k) = \frac{k h_\nu^{\prime\text{out}}(kr)}{h_\nu^{\text{out}}(kr)} \Psi_{\nu\mu}^{\text{ext}}(r, k). \tag{20}$$

To relate (20) with the radially extrapolated field $\partial \mathcal{P}_{\nu\mu}^{\text{ff}}$ in (10), the following continuity condition on open $\mathcal{B}$ is chosen:

$$\Psi_{\nu\mu}^{\text{int}}(b, k) = \frac{1}{2} \mathcal{P}_{\nu\mu}^{\text{ff}}(b, k) = \frac{1}{2} \frac{h_\nu^{\text{out}}(kb)}{k h_\nu^{\prime\text{out}}(kb)} \partial \mathcal{P}_{\nu\mu}^{\text{ff}}(b, k),$$

$$\Psi_{\nu\mu}^{\text{ext}}(b, k) = \frac{1}{2} \mathcal{P}_{\nu\mu}^{\text{ff}}(b, k) = \frac{1}{2} \frac{h_\nu^{\text{out}}(kb)}{k h_\nu^{\prime\text{out}}(kb)} \partial \mathcal{P}_{\nu\mu}^{\text{ff}}(b, k). \tag{21}$$

Combining (21) with (20) leads to

$$\partial \Psi_{\nu\mu}^{\text{int}}(b, k) = \frac{1}{2} \frac{h_\nu^{\prime\text{in}}(kb)}{h_\nu^{\text{in}}(kb)} \frac{h_\nu^{\text{out}}(kb)}{h_\nu^{\prime\text{out}}(kb)} \partial \mathcal{P}_{\nu\mu}^{\text{ff}}(b, k),$$

$$\partial \Psi_{\nu\mu}^{\text{ext}}(b, k) = \frac{1}{2} \partial \mathcal{P}_{\nu\mu}^{\text{ff}}(b, k). \tag{22}$$

Finally, (13), (14), and (15) are obtained by substituting (22) in (17), by using the Wronskian relation

$$h_\nu^{\prime\text{in}}(kb) h_\nu^{\text{out}}(kb) - h_\nu^{\text{in}}(kb) h_\nu^{\prime\text{out}}(kb) = \frac{-2j}{(kb)^2}, \tag{23}$$

and by further restricting the action of resulting open boundary filters $\mathcal{O}_\nu$ to affect only the magnitude response of $\mathcal{F}_\nu^{\text{RF}}$.

No assumption on $\mathcal{A}$ was required to formulate $\mathcal{O}_\nu$ in (14). These filters can hence be used to modify the low-frequency content of SBMFs for any other boundary condition on $\mathcal{A}$.

Figure 4 shows examples of $\mathcal{O}_\nu$ for distinct orders ν. It is observed that these filters attenuate high-order components at lower frequencies. Analogous low-frequency decay with
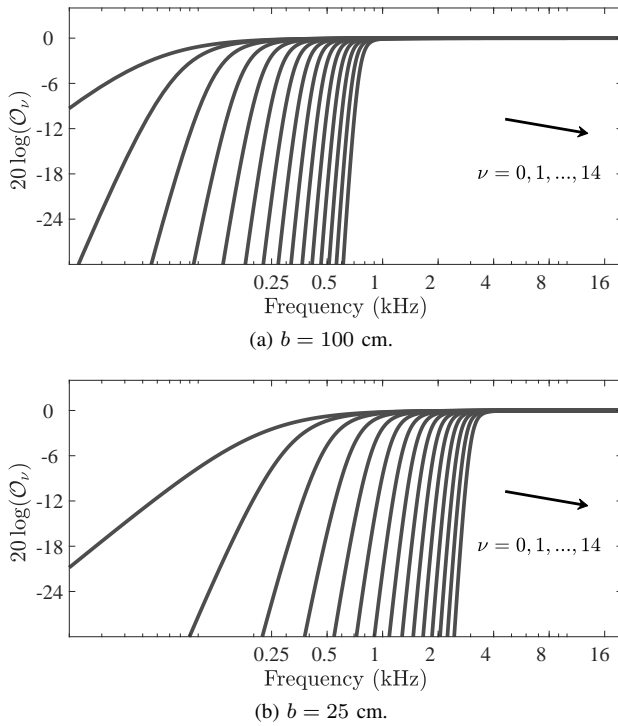
(a) $b = 100$ cm.

(b) $b = 25$ cm.

Fig. 4. Proposed open boundary filters $\mathcal{O}_\nu$ in (14) for gain limitation.

increasing order is empirically observed when the radiation from multipole sources is characterized [54].

Figure 5 presents examples of $\mathcal{F}_\nu^{\mathrm{RI}}$ in (7), $\mathcal{F}_\nu^{\mathrm{RF}}$ in (8), and $\mathcal{F}_\nu^{\mathrm{RO}}$ in (15) for different orders ν. The highest order $\nu = 14$ and the microphone radius $a = 8.5$ cm used in examples hereafter correspond to the 252-channel recording system reported in [27], [28]. Excessive gains in lower frequencies at high orders are observed in $\mathcal{F}_\nu^{\mathrm{RI}}$ and $\mathcal{F}_\nu^{\mathrm{RF}}$ as a consequence of the ill-posedness of inversion. Such difficulty at lower frequencies is not observed in $\mathcal{F}_\nu^{\mathrm{RO}}$ thanks to the use of the gain-limiting filters $\mathcal{O}_\nu$. In addition, for large values of ν, local maxima of $|\mathcal{F}_\nu^{\mathrm{RO}}|$ are well localized and occur when $\nu \approx kb$, whereas local minima occur when $\nu \approx ka$. This can be verified by using the first-derivative test.

Note also in Fig. 5 that gains of $\mathcal{F}_\nu^{\mathrm{RO}}$ at middle frequencies still increase with increasing order. To make high-order SBMFs suitable for high-resolution microphone arrays, gain-limitation methods are addressed in the next section in the context of order truncation, that is, considering signals of limited angular bandwidths.

IV. ANGULAR BANDWIDTH LIMITATION

The effects of representing spherical signals within angular spectra of limited bandwidth are investigated by distinguishing the finite-sum part of (2) up to a maximum order N and the residual terms. Explicitly,

$$\Psi = \Psi_N^{\mathrm{band}} + \varepsilon_N, \tag{24}$$

in which the band-limited component is defined by

$$\Psi_N^{\mathrm{band}}(\vec{r}, k) = \sum_{\nu=0}^{N} \sum_{\mu=-\nu}^{\nu} \mathcal{T}_{\nu\mu}(b, \vec{r}, k) \mathcal{F}_\nu(a, b, k) \mathcal{P}_{\nu\mu}(a, k), \tag{25}$$

and ε_N comprises all residual terms of order $\nu \geq N + 1$.

The action of $\mathcal{F}_\nu$ in limited bandwidths is examined by substituting (3) and (5) in (25). Swapping integrals and sums by virtue of their absolute convergence yields a recasting of (25) as the integral form

$$\Psi_N^{\mathrm{band}}(\vec{r}, k) = \int_{\Omega_a \in \mathcal{A}} \int_{\Omega_b \in \mathcal{B}} \mathcal{C}_N(\vec{a}, \vec{b}, k) \times \\ \mathcal{T}(\vec{b}, \vec{r}, k) \mathcal{P}(\vec{a}, k) d\Omega_b d\Omega_a, \tag{26}$$

where the band-limited matching function between $\vec{a}$ and $\vec{b}$ is

$$\mathcal{C}_N(\vec{a}, \vec{b}, k) = \sum_{\nu=0}^{N} \frac{2\nu + 1}{4\pi} \mathcal{F}_\nu(a, b, k) P_\nu(\cos \Theta_{\vec{a}\vec{b}}). \tag{27}$$

Owing to the addition theorem [4], the angular part of $\mathcal{C}_N$ in (27) is described by the non-normalized Legendre polynomial P_ν of order ν, evaluated at the angle $\Theta_{\vec{a}\vec{b}}$ between $\vec{a}$ and $\vec{b}$. The radial part of $\mathcal{C}_N$ is exclusively described by $\mathcal{F}_\nu$.

High orders involve high-gain SBMFs (see Fig. 5). Two existing general-purpose gain-limitation methods for use with $\mathcal{F}_\nu^{\mathrm{RI}}$ and $\mathcal{F}_\nu^{\mathrm{RF}}$ are described below in sections IV-A and IV-B. A new gain-limitation method for use with the proposed $\mathcal{F}_\nu^{\mathrm{RO}}$ is then presented in section IV-C. The time-domain effects due to the use of each gain-limited SBMF will be exemplified relying on the impulse responses of $\mathcal{C}_N$ in (27).

A. Frequency-dependent gain-limited RI- and RF-SBMFs

Excessive gains are overcome by imposing frequency-dependent maximum orders N_k beyond which the contributions of SBMFs are simply discarded according to

$$\mathcal{F}_\nu^{\mathrm{trunc}} = \begin{cases} \mathcal{F}_\nu, & \nu \leq N_k, \\ 0, & \text{otherwise.} \end{cases} \tag{28}$$

Here, $\mathcal{F}_\nu$ represents one of the filters in (7) or (8).

Determination of the maximum orders so as to pursue a maximum reconstruction radius equal to the reproduction radius b is equivalent to using the far-to-near field transitions [4]:

$$N_k = \lfloor kb \rfloor. \tag{29}$$

The black square markers in Fig. 5 exemplify maximum gains of $\mathcal{F}_\nu^{\mathrm{RFtrunc}}$ based on (8), (28), and (29). Below such maxima, gains at lower frequencies are set to zero. High gains are still required at middle frequencies when the attempt is made to cover large reconstruction radii with higher orders.

Maximum orders can also be set by assuming residuals in (24) approximately equal to a constant $\hat{\varepsilon}_N$, resulting in [46]

$$N_k = \left\lfloor \left\{ \left[ka + \frac{1}{2} \left(3 \ln \frac{1}{\hat{\varepsilon}_N} + \frac{1}{2} \ln (ka) \right)^{\frac{2}{3}} (ka)^{\frac{1}{3}} \right]^4 + \\ \left[\frac{1}{\ln \left(\frac{b}{a} \right)} \ln \left(\frac{\left(\frac{b}{a} \right)^{\frac{3}{2}}}{\left(\frac{b}{a} - 1 \right)^{\frac{3}{2}} \hat{\varepsilon}_N} \right) + 1 \right]^4 \right\}^{\frac{1}{4}} \right\rfloor. \tag{30}$$
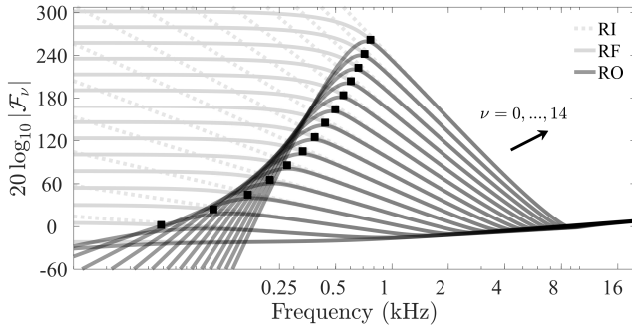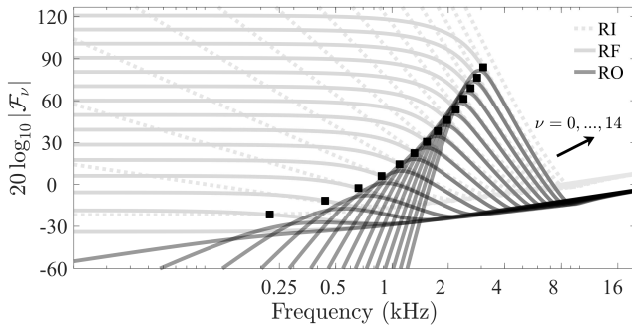
(a) $a = 8.5$ cm, $b = 100$ cm.

(b) $a = 8.5$ cm, $b = 25$ cm.

Fig. 5. Gains of existing filters $\mathcal{F}_\nu^{\mathrm{RI}}$ in (7) and $\mathcal{F}_\nu^{\mathrm{RF}}$ in (8), and proposed filters $\mathcal{F}_\nu^{\mathrm{RO}}$ in (15), for different orders ν. Excessive gains at higher orders and lower frequencies are observed in $\mathcal{F}_\nu^{\mathrm{RI}}$ and $\mathcal{F}_\nu^{\mathrm{RF}}$. Gains of $\mathcal{F}_\nu^{\mathrm{RO}}$ are bounded at lower frequencies because of the use of the filters $\mathcal{O}_\nu$ shown in Fig. 4. Black square markers ■ indicate values at the transitions between the far- and near-field regions described by $\nu = kb$. These transitions constitute the frequency-dependent gain-limiting thresholds in (29) that pursue a maximum reconstruction radius equal to the reproduction radius b. Maxima of $|\mathcal{F}_\nu^{\mathrm{RO}}|$ smoothly reach the far-to-near transition values.

(a) $a = 8.5$ cm, $b = 100$ cm.

(b) $a = 8.5$ cm, $b = 25$ cm.

Fig. 6. Gain-limited SBMFs: proposed $\mathcal{F}_\nu^{\mathrm{ROlim}}$ in (32) for maximum gain $20 \log_{10} \gamma = 40$, and existing $\mathcal{F}_\nu^{\mathrm{RFreg}}$ in (31) for regularization parameter $\lambda = 5 \times 10^{-3}$. Filters $\mathcal{F}_\nu^{\mathrm{ROlim}}$ conveniently confine the action of gain limitation to the higher orders and frequencies, in contrast to filters $\mathcal{F}_\nu^{\mathrm{RFreg}}$, whose action extents to the lower orders and frequencies where gain limitation is not required. In addition, black square markers ■ indicate maximum gains of existing $\mathcal{F}_\nu^{\mathrm{RFtrunc}}$ based on (28) and (30) for order truncation error $\hat{\varepsilon}_N = 2 \times 10^{-2}$. A comparisson of maximum gains and markers indicates that the order truncation error is also held nearly constant when using $\mathcal{F}_\nu^{\mathrm{ROlim}}$.

Figure 6 shows examples of gain-limited SBMFs. The black square markers illustrate the maximum gains of $\mathcal{F}_\nu^{\mathrm{RFtrunc}}$ based on (8), (28), and (30). Below such maxima, gains at lower frequencies are set to zero. Gains are thus kept approximately constant and bounded, and the action of high-order components is restricted to the higher frequencies. Nevertheless, frequency-dependent order truncation generally produces discontinuities along frequency that strongly affect the time-domain behavior.

Figure 7 illustrates the time-domain effects of using gain-limited SBMFs in terms of the rectified impulse responses of the band-limited matching function $\mathcal{C}_N$ in (27). Impulse responses were calculated by applying the one-dimensional inverse Fourier transform to the conjugate symmetric vector that corresponds to the frequency discretization of $\mathcal{C}_N$. Discretization was performed by using a sampling frequency of 48 kHz and a frame of 512 samples. These values were intended to ensure the visualization of sound propagation along the distances under consideration.

It is observed in Figs. 7b and 7f that, when $\mathcal{F}_\nu^{\mathrm{RFtrunc}}$ is used, discontinuities along frequency produce impulse responses affected by undesired replicas of main peaks.
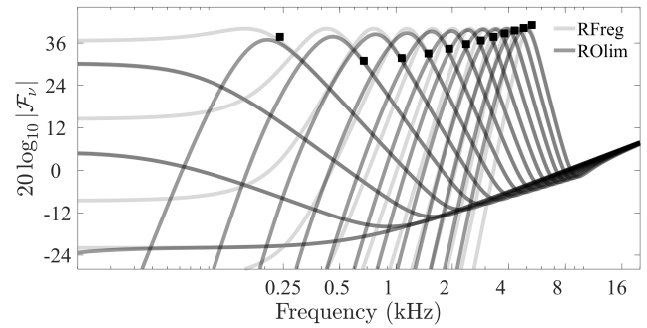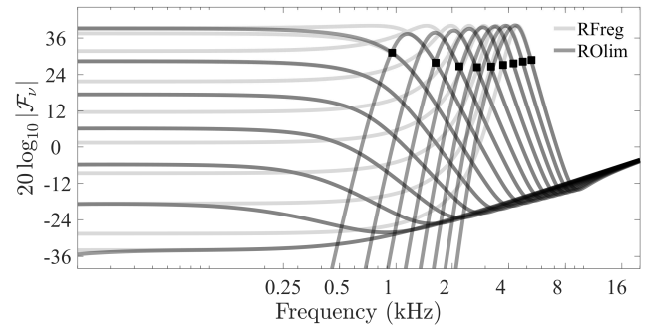
B. Regularization-based gain-limited RI- and RF-SBMFs

Tikhonov regularization [56] enables gain limitation without the need for frequency-dependent order truncation and, hence, without producing discontinuities along frequency. Regularization is equivalent to applying the regularized filter

$$\mathcal{F}_\nu^{\mathrm{reg}} = \frac{\mathcal{F}_\nu}{1 + \lambda^2 |\mathcal{F}_\nu|^2}, \tag{31}$$

where $\mathcal{F}_\nu$ is one of the filters in (7) or (8), and λ is the regularization parameter. Derivation of (31) is detailed in appendix C. Similar formulas appear in [9], [18], [19], [30]–[32].

Examples of $\mathcal{F}_\nu^{\mathrm{RFreg}}$ based on (8) and (31) are shown in Fig. 6. Smooth and bounded gains are produced as a consequence of applying (31) over all frequencies at once. In the time domain, a substantial reduction of main peak replicas is achieved at the cost of a slight dispersion of concentration around main peaks as can be observed in Figs. 7c and 7g.

When (31) is used, the effects of regularizing the high-order components extend to the range of lower frequencies, as is further observed in Fig. 6. Lower frequencies, however, are sufficiently covered with lower orders. This observation motivates an alternative gain-limitation method, presented in the next section.
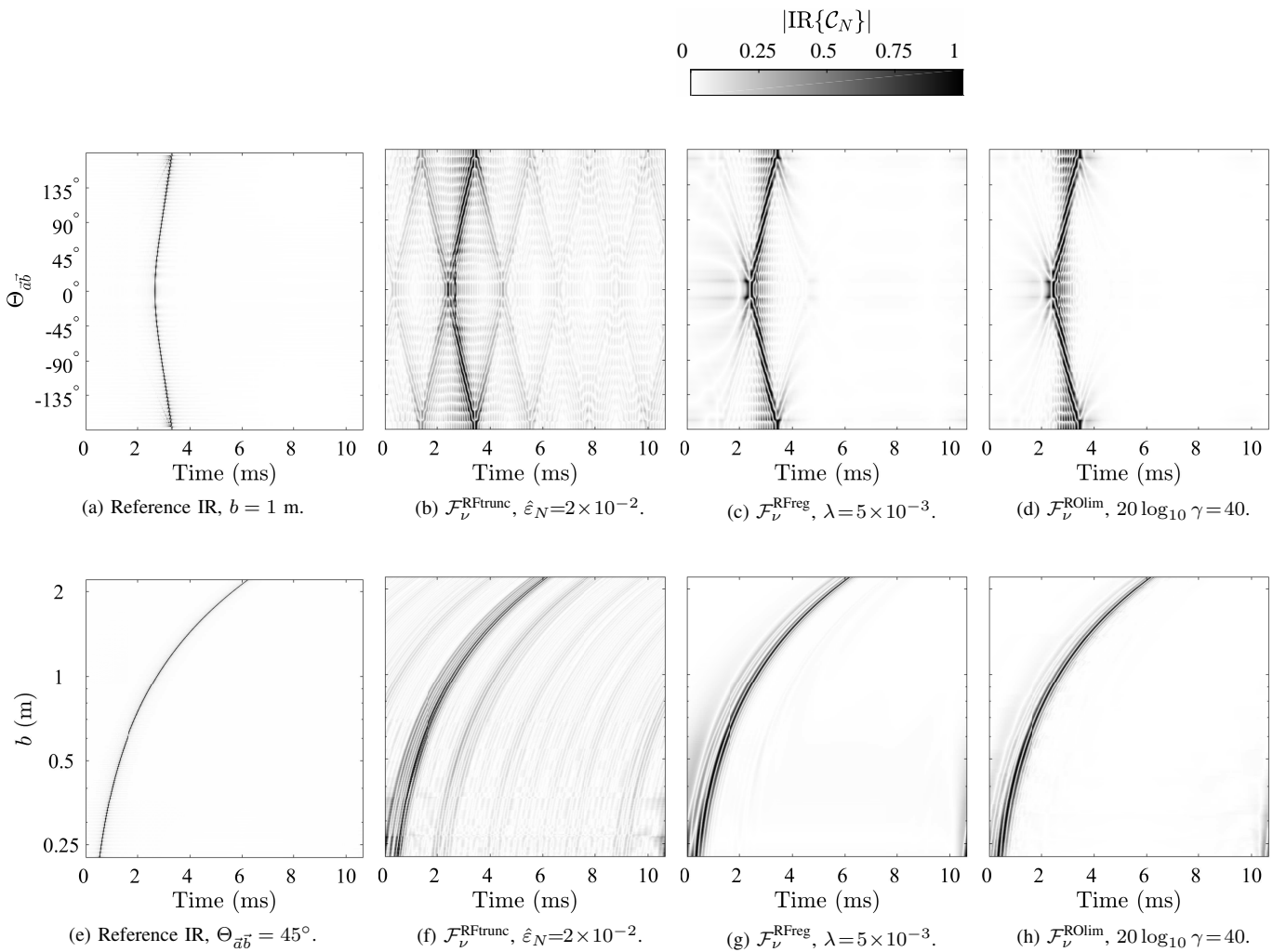
Fig. 7.   Time-domain effects of angular band limitation illustrated in terms of absolute values of normalized impulse responses (IRs) of $\mathcal{C}_N$ in (27), for $N = 14$ and $a = 8.5$ cm. Top panels correspond to IRs for a single reproduction radius $b = 1$ m and different angles $\Theta_{\vec{ab}}$ between recording and reproduction points, whereas bottom panels correspond to IRs for a single angle $\Theta_{\vec{ab}} = 45°$ and different reproduction radii b. Panels (a) and (e) correspond to normalized reference IRs obtained by spatial-domain inversion of the acoustically rigid sphere transfer functions [55], which can be considered to be band-unlimited. Panels (b), (c), (d), (f), (g), and (h) correspond to the IRs of $\mathcal{C}_N$ in (27) obtained using the following gain-limited filters: $\mathcal{F}_\nu^{\text{RFtrunc}}$ in (28) and (30), $\mathcal{F}_\nu^{\text{RFreg}}$ in (31), and $\mathcal{F}_\nu^{\text{ROlim}}$ in (32). Results using $\mathcal{F}_\nu^{\text{ROlim}}$ shown in panels (d) and (h) present the most localized responses around the maximum values of $\mathcal{C}_N$.

C. Gain-limited RO-SBMFs

The SBMFs proposed in (15) provide a suitable basis for designing gain-limited SBMFs because their relative maximum gains are well localized in frequency and constitute a smooth transition from the far to the near fields (see Fig. 5). For every order ν, new maxima below a limit γ can be achieved by shifting the original maxima toward the higher frequencies. This is possible, in turn, when imposing smaller maximum reconstruction radii $\varrho_\nu(\gamma)$. Gain-limited SBMFs are thus defined by

$$\mathcal{F}_\nu^{\text{ROlim}}(a, b, \varrho_\nu, k) = \mathcal{O}_\nu(\varrho_\nu, k) \times \mathcal{F}_\nu^{\text{RF}}(a, b, k). \quad (32)$$

The open boundary filters $\mathcal{O}_\nu$ introduced in (14) are used here with maximum reconstruction radii calculated according to

$$\varrho_\nu(\gamma) = \sigma_0 \frac{\nu + \nu_0}{k_\gamma}, \quad (33)$$

where k_γ is the wave number at which the prescribed maximum gain γ occurs, and it is found in such a way that

$$k_\gamma : |\mathcal{F}_\nu^{\text{RF}}(a, b, k_\gamma)| = \gamma. \quad (34)$$

Additional parameters σ_0 and ν_0 are introduced to compensate for possible inaccuracies when placing the new relative maxima. We have empirically verified that it is enough to set $\sigma_0 = 0.98$ and $\nu_0 = 0.5$ for all cases involving orders $\nu \leq 43$.

Examples of $\mathcal{F}_\nu^{\text{ROlim}}$ based on (32) are shown in Fig. 6. Smooth-and-bounded-gain SBMFs are obtained when the reconstruction radius is decreased according to (33). The action of high orders is conveniently confined to high-frequency bands. Moreover, the impulse responses of $\mathcal{C}_N$ in (27) are slightly more localized around the main peaks, as can be observed when contrasting Figs. 7d and 7h, respectively, with Figs. 7c and 7g.

V. SPATIAL DISCRETIZATION

In limited angular bandwidths, obtaining Ψ_N^{band} in (25) involves the approximation of $\mathcal{P}_{\nu\mu}$ in (5) for a finite number M of microphones on $\mathcal{A}$, and the approximation of $\mathcal{T}_{\nu\mu}$ in (3) for a finite number L of loudspeakers on $\mathcal{B}$. This section shows that Ψ_N^{band} consists of an approximation component after spatial discretization, denoted by $\Psi_{N;M,L}^{\text{disc}}$, and three residual components denoted by ε_M, ε_L, and $\varepsilon_{M,L}$. Explicitly,

$$\Psi_N^{\text{band}} = \Psi_{N;M,L}^{\text{disc}} + \varepsilon_M + \varepsilon_L + \varepsilon_{M,L}. \qquad (35)$$

Here, ε_M describes the isolated effects of sampling on $\mathcal{A}$, ε_L describes the isolated effects of sampling on $\mathcal{B}$, and $\varepsilon_{M,L}$ describes the coupled effects of sampling on $\mathcal{A}$ and $\mathcal{B}$. Similar terms have recently been identified in [45].

The terms in (35) also allow definition of the following residual-to-signal ratios:

$$E_M = \frac{\|\varepsilon_M\|}{\|\Psi\|}, \;\; E_L = \frac{\|\varepsilon_L\|}{\|\Psi\|}, \;\; E_{M,L} = \frac{\|\varepsilon_{M,L}\|}{\|\Psi\|}, \qquad (36)$$

where Ψ denotes a target band-unlimited sound pressure field, and $\|\cdot\|$ denotes the 2-norm along $\vec{r}$ in the interior volume. These residual-to-signal ratios are relative errors to evaluate the overall sampling effects as a function of frequency.

In unlimited angular bandwidths, the residual term ε_N in (24) would need to be included into the spatial discretization analyses. Rigorous studies on the effects of sampling ε_N have been separately conducted for microphone [11], [12] and loudspeaker [40] arrays. Such effects are referred to as spatial aliasing, and have been found to be more prominent at higher frequencies. Because the focus of this research is the assessment of SBMFs at lower and middle frequencies, analyses are restricted hereafter to limited bandwidths. However, because the total reconstruction error can be writen as

$$\Psi - \Psi_{N;M,L}^{\text{disc}} = \varepsilon_M + \varepsilon_L + \varepsilon_{M,L} + \varepsilon_N, \qquad (37)$$

as deduced from (24) and (35), all isolated and combined contributions of spatial aliasing on $\mathcal{A}$ and $\mathcal{B}$ are hence considered in the total error, given that ε_N is part of (37).

Section V-A derives analytical expressions for each term in (35) by analyzing how orthonormality in (53) is affected by numerical integration over $\mathcal{A}$ and $\mathcal{B}$. Finally, using (35) and (36), section V-B exemplifies how sound field reconstruction based on SBMFs is affected by band limitation and sampling.

A. Discrete-space analysis based on orthonormality

Let $\{\Omega_m, \alpha_m\}_{m=1,\cdots,M}$ be a sampling scheme of $\mathcal{A}$, where Ω_m are measurement nodes and α_m are integration weights. Similarly, let $\{\Omega_\ell, \beta_\ell\}_{\ell=1,\cdots,L}$ be a sampling scheme of $\mathcal{B}$, where Ω_ℓ are secondary nodes and β_ℓ are integration weights.

Numerical integration of (53) over $\mathcal{A}$ and $\mathcal{B}$ respectively define the orthonormality residuals $\epsilon_{\nu\nu'\mu\mu'}^{(M)}$ and $\epsilon_{\nu\nu''\mu\mu''}^{(L)}$ by

$$\underbrace{\int_{\Omega_a \in \mathcal{A}} Y_\nu^\mu(\Omega_a)\overline{Y_{\nu'}^{\mu'}(\Omega_a)}d\Omega_a}_{\delta_{\nu\nu'\mu\mu'}^{(\mathcal{A})}} = \underbrace{\sum_{m=1}^{M} Y_\nu^\mu(\Omega_m)\overline{Y_{\nu'}^{\mu'}(\Omega_m)}\alpha_m}_{\Delta_{\nu\nu'\mu\mu'}^{(M)}} + \epsilon_{\nu\nu'\mu\mu'}^{(M)}, \qquad (38)$$

$$\underbrace{\int_{\Omega_b \in \mathcal{B}} Y_\nu^\mu(\Omega_b)\overline{Y_{\nu''}^{\mu''}(\Omega_b)}d\Omega_b}_{\delta_{\nu\nu''\mu\mu''}^{(\mathcal{B})}} = \underbrace{\sum_{\ell=1}^{L} Y_\nu^\mu(\Omega_\ell)\overline{Y_{\nu''}^{\mu''}(\Omega_\ell)}\beta_\ell}_{\Delta_{\nu\nu''\mu\mu''}^{(L)}} + \epsilon_{\nu\nu''\mu\mu''}^{(L)}. \qquad (39)$$

In addition, band-limited signals are modeled in transform domain by relying on the Kronecker delta sifting property:

$$\mathcal{P}_{\nu\mu} = \sum_{\nu',\mu'}^{N'} \mathcal{P}_{\nu'\mu'}\delta_{\nu\nu'\mu\mu'}^{(\mathcal{A})}, \;\; \mathcal{T}_{\nu\mu} = \sum_{\nu'',\mu''}^{N''} \mathcal{T}_{\nu''\mu''}\delta_{\nu\nu''\mu\mu''}^{(\mathcal{B})}. \qquad (40)$$

For simplicity, the abbreviations $\sum_{\nu,\mu}^{N} \equiv \sum_{\nu=0}^{N}\sum_{\mu=-\nu}^{\nu}$ and $\delta_{\nu\nu'\mu\mu'} = \delta_{\nu\nu'}\delta_{\mu\mu'}$ are used hereafter.

Several sampling theorems on the sphere that relate a finite bandwidth and a sampling resolution exist in the literature (e.g., [57]). In general, it is assumed here that

$$\begin{aligned} (N'+1)^2 &\leq M, \\ (N''+1)^2 &\leq L, \\ N &= \min(N', N''). \end{aligned} \qquad (41)$$

Equating (40) and (25) produces

$$\Psi_N^{\text{band}} = \sum_{\nu,\mu}^{N}\sum_{\nu',\mu'}^{N'}\sum_{\nu'',\mu''}^{N''} \mathcal{T}_{\nu''\mu''}\mathcal{F}_\nu\mathcal{P}_{\nu'\mu'}\delta_{\nu\nu'\mu\mu'}^{(\mathcal{A})}\delta_{\nu\nu''\mu\mu''}^{(\mathcal{B})}. \qquad (42)$$

On the other hand, from the calculation of $\Delta_{\nu\nu'\mu\mu'}^{(M)} \times \Delta_{\nu\nu''\mu\mu''}^{(L)}$ based on (38) and (39), it follows that

$$\begin{aligned} \delta_{\nu\nu'\mu\mu'}^{(\mathcal{A})}\delta_{\nu\nu''\mu\mu''}^{(\mathcal{B})} &= \Delta_{\nu\nu'\mu\mu'}^{(M)}\Delta_{\nu\nu''\mu\mu''}^{(L)} + \\ \delta_{\nu\nu'\mu\mu'}^{(\mathcal{A})}\epsilon_{\nu\nu''\mu\mu''}^{(L)} &+ \delta_{\nu\nu''\mu\mu''}^{(\mathcal{B})}\epsilon_{\nu\nu'\mu\mu'}^{(M)} - \epsilon_{\nu\nu'\mu\mu'}^{(M)}\epsilon_{\nu\nu''\mu\mu''}^{(L)}. \end{aligned} \qquad (43)$$

The terms on the right side of (35) arise when (43) is replaced in (42). The approximation component in (35) is therefore defined by

$$\Psi_{N;M,L}^{\text{disc}} = \sum_{\nu,\mu}^{N}\sum_{\nu',\mu'\nu'',\mu''}^{N'} \mathcal{T}_{\nu''\mu''}\mathcal{F}_\nu\mathcal{P}_{\nu'\mu'}\Delta_{\nu\nu'\mu\mu'}^{(M)}\Delta_{\nu\nu''\mu\mu''}^{(L)}, \qquad (44)$$

whereas the residual terms in (35) that describe the effects of sampling are correspondingly defined by

$$\varepsilon_M = \sum_{\nu,\mu}^{N}\sum_{\nu',\mu'}^{N'} \mathcal{T}_{\nu\mu}\mathcal{F}_\nu\mathcal{P}_{\nu'\mu'}\epsilon_{\nu\nu'\mu\mu'}^{(M)}, \qquad (45)$$

$$\varepsilon_L = \sum_{\nu,\mu}^{N}\sum_{\nu'',\mu''}^{N''} \mathcal{T}_{\nu''\mu''}\mathcal{F}_\nu\mathcal{P}_{\nu\mu}\epsilon_{\nu\nu''\mu\mu''}^{(L)}, \qquad (46)$$

and

$$\varepsilon_{M,L} = -\sum_{\nu,\mu}^{N}\sum_{\nu',\mu'\nu'',\mu''}^{N'} \mathcal{T}_{\nu''\mu''}\mathcal{F}_\nu\mathcal{P}_{\nu'\mu'}\epsilon_{\nu\nu'\mu\mu'}^{(M)}\epsilon_{\nu\nu''\mu\mu''}^{(L)}. \qquad (47)$$

$$|\Delta^{(M)}_{\nu\nu'\mu\mu'} \times \Delta^{(L)}_{\nu\nu''\mu\mu''}|$$

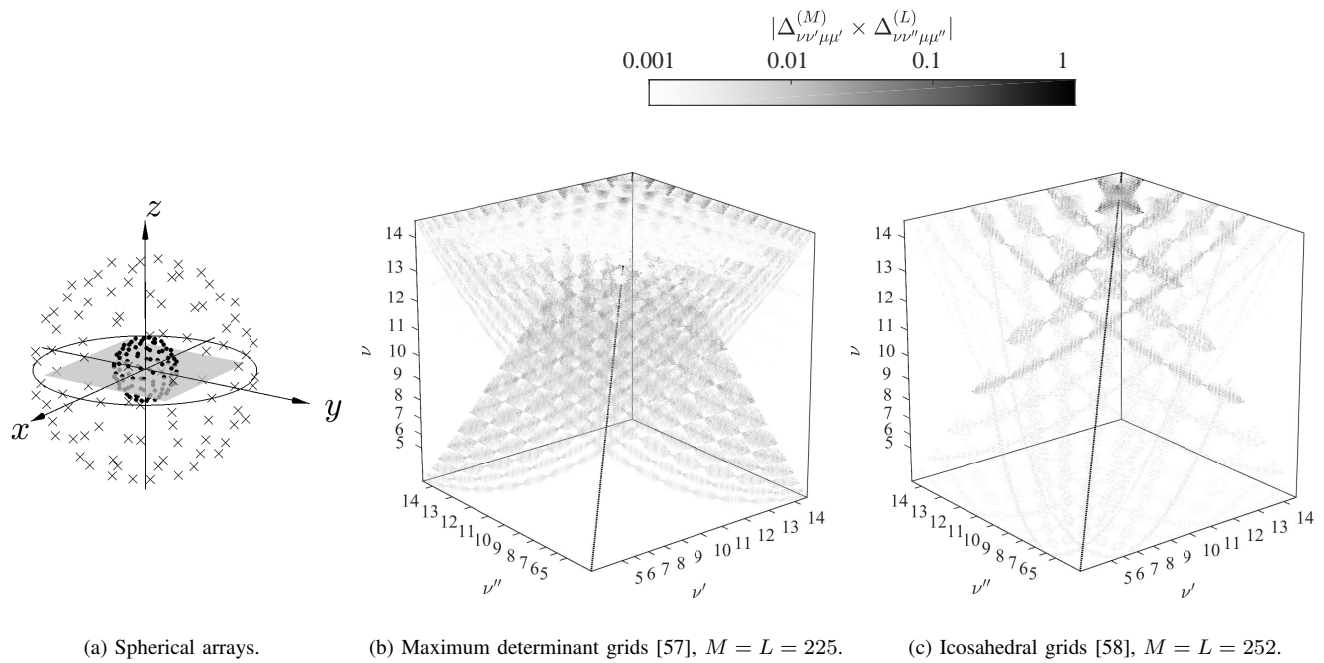(a) Spherical arrays. (b) Maximum determinant grids [57], $M = L = 225$. (c) Icosahedral grids [58], $M = L = 252$.

Fig. 8. Geometry used to illustrate the effects of spatial sampling in sound field reconstruction on a region of the xy-plane. In diagram (a), not shown to scale, dots indicate microphones, marks indicate loudspeakers, and the gray plane is the reconstruction region. Patterns $\Delta^{(M)}_{\nu\nu'\mu\mu'} \Delta^{(L)}_{\nu\nu''\mu\mu''}$ affecting reconstruction in (44) are shown for maximum determinant (b) and icosahedral (c) grids. In icosahedral grids, sampling effects are more sparsely distributed along order.

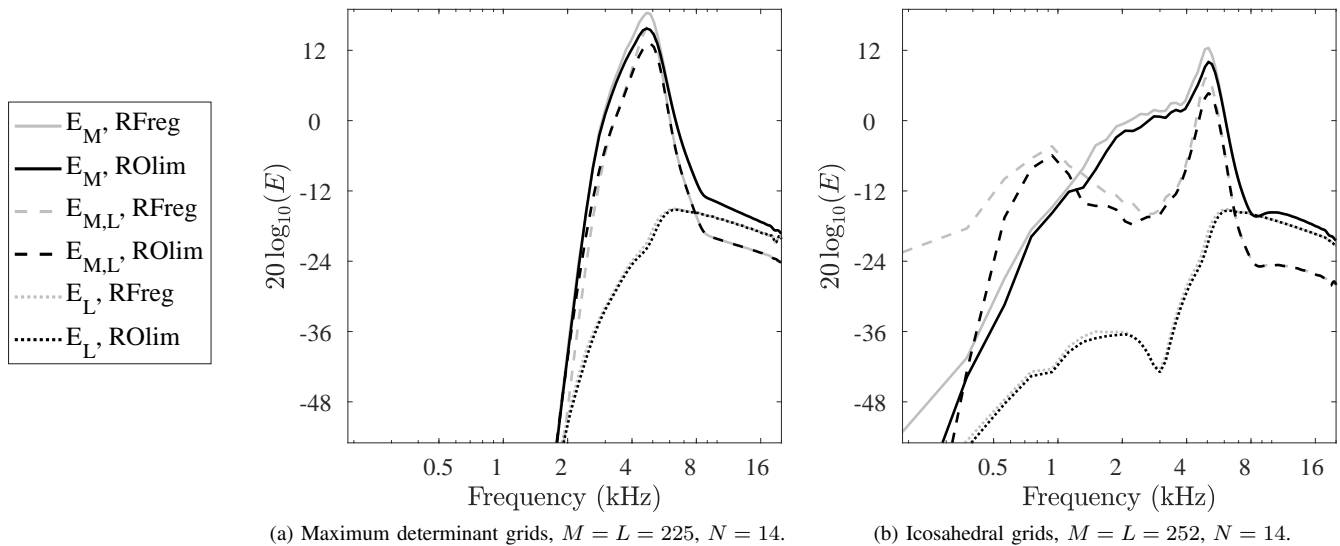(a) Maximum determinant grids, $M = L = 225$, $N = 14$. (b) Icosahedral grids, $M = L = 252$, $N = 14$.

Fig. 9. Overall sampling effects on the reconstruction region calculated in terms of the residual-to-signal ratios E_M (isolated effects of sampling the recording boundary with M microphones), E_L (isolated effects of sampling the reproduction boundary with L loudspeakers), and $E_{M,L}$ (coupled effects of sampling the recording and reproduction boundaries). E_M, E_L, and $E_{M,L}$ are defined in (36). In general, the values of E_M and $E_{M,L}$ are more prominent than E_L. Results are shown for maximum determinant (a) and icosahedral (b) grids. SBMFs $\mathcal{F}^{\mathrm{RFreg}}_\nu$ use a regularization parameter $\lambda = 5 \times 10^{-3}$, whereas $\mathcal{F}^{\mathrm{ROlim}}_\nu$ use a maximum gain $20\log_{10}\gamma = 40$. The single point source is at $\vec{r}_{\mathrm{source}} = (x_{\mathrm{source}}, y_{\mathrm{source}}, z_{\mathrm{source}}) = (0, 50, 0)$ cm. Reconstruction is done on $\vec{r}$ in a 40×40 cm^2 region on the xy-plane, for $a = 8.5$ cm and $b = 50$ cm.

B. Effects of sampling in sound field reconstruction

Reconstruction of a band-unlimited target field Ψ at $\vec{r} = (r, \Omega)$ that emanates from a point source at $\vec{r}_{\mathrm{source}} = (r_{\mathrm{source}}, \Omega_{\mathrm{source}})$ is addressed to exemplify the effects of sampling. The target field reads

$$\Psi(\vec{r}, k) = \frac{\exp(jk|\vec{r} - \vec{r}_{\mathrm{source}}|)}{|\vec{r} - \vec{r}_{\mathrm{source}}|}. \tag{48}$$

Continuous-space recordings $\mathcal{P}$ on $\vec{a} \in \mathcal{A}$ due to a single source at $\vec{r}_{\mathrm{source}}$ are modeled in terms of their SFT on $\mathcal{A}$ as

$$\mathcal{P}_{\nu'\mu'}(a, \vec{r}_{\mathrm{source}}, k) = \frac{-4\pi h^{\mathrm{out}}_{\nu'}(kr_{\mathrm{source}})\overline{Y^{\mu'}_{\nu'}(\Omega_{\mathrm{source}})}}{ka^2 h'^{\mathrm{out}}_{\nu'}(ka)}. \tag{49}$$

Similarly, the free-field transfer functions $\mathcal{T}^{\mathrm{ff}}$ from $\mathcal{B}$ to $\vec{r}$ are modeled in terms of their SFT on $\mathcal{B}$ as

$$\mathcal{T}^{\mathrm{ff}}_{\nu''\mu''}(b, \vec{r}, k) = -4\pi jk h^{\mathrm{in}}_{\nu''}(kb) \mathrm{j}_{\nu''}(kr) Y^{\mu''}_{\nu''}(\Omega), \tag{50}$$

where j_ν denotes the spherical Bessel function of order ν.
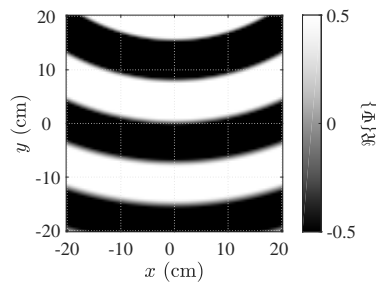
(a) Ψ in (48) due to a single point source located at $\vec{r}_{\text{source}} = (x_{\text{source}}, y_{\text{source}}, z_{\text{source}}) = (0, 50, 0)$ cm, for 2250 Hz.

(b) Ψ_N^{band} in (25), $\mathcal{F}_\nu^{\text{RFreg}}$.   (c) $\Psi_{N;M,L}^{\text{disc}}$ in (44).   (d) ε_M in (45).   (e) ε_L in (46).   (f) $\varepsilon_{M,L}$ in (47).   (g) $\Psi - \Psi_{N;M,L}^{\text{disc}}$.

(h) Ψ_N^{band} in (25), $\mathcal{F}_\nu^{\text{ROlim}}$.   (i) $\Psi_{N;M,L}^{\text{disc}}$ in (44).   (j) ε_M in (45).   (k) ε_L in (46).   (l) $\varepsilon_{M,L}$ in (47).   (m) $\Psi - \Psi_{N;M,L}^{\text{disc}}$.
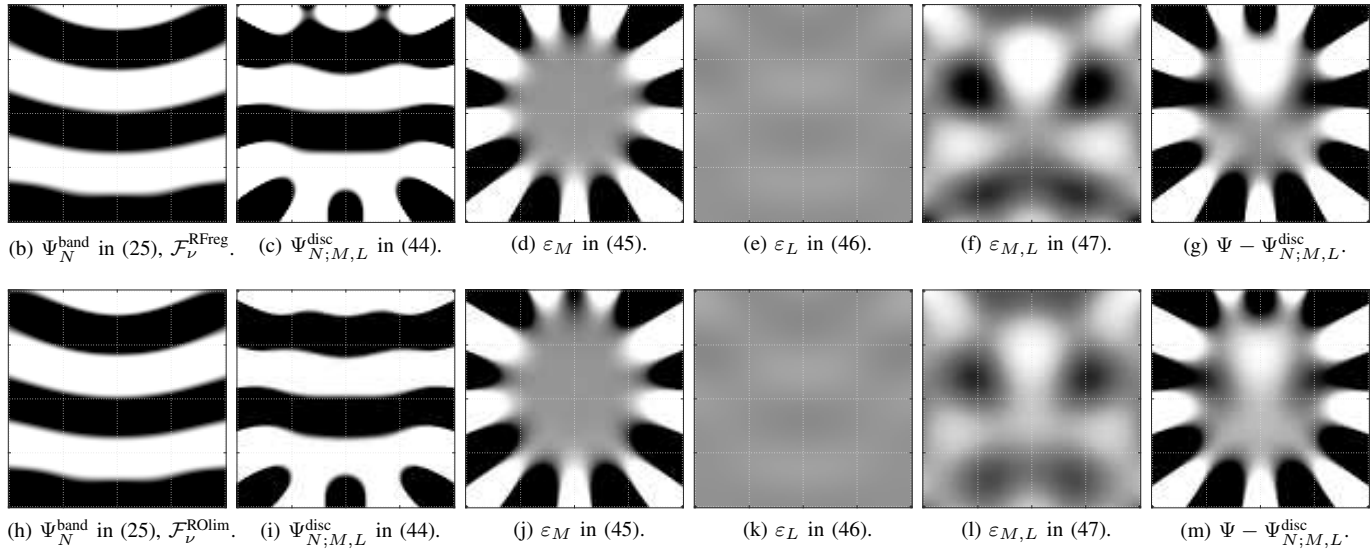
Fig. 10.   Local effects of band limitation and sampling upon reconstruction of the target band-unlimited pressure field Ψ in (a) by using icosahedral grids. Band-limited pressure fields Ψ_N^{band} are shown in panels (b) and (h), whereas reconstructed pressure fields $\Psi_{N;M,L}^{\text{disc}}$ are shown in panels (c) and (i). Recall from (24) and (35) that $\Psi = \Psi_N^{\text{band}} + \varepsilon_N$, and $\Psi_N^{\text{band}} = \Psi_{N;M,L}^{\text{disc}} + \varepsilon_M + \varepsilon_L + \varepsilon_{M,L}$, where ε_M denotes the isolated sampling effects of recording shown in panels (d) and (j), ε_L denotes the isolated sampling effects of reproduction shown in panels (e) and (k), and $\varepsilon_{M,L}$ denotes the coupled sampling effects of recording and reproduction shown in panels (f) and (l). Note also that the total errors in panels (g) and (m) comprise the residual ε_N. Real parts of all these components are shown. Panels (b)–(g) correspond to reconstruction with $\mathcal{F}_\nu^{\text{RFreg}}$, whereas panels (h)–(m) correspond to $\mathcal{F}_\nu^{\text{ROlim}}$. The use of $\mathcal{F}_\nu^{\text{ROlim}}$ extends the reconstruction area thanks to the reductions of ε_M and $\varepsilon_{M,L}$; this is confirmed by comparing (d) with (j), (f) with (l), and (g) with (m).

Figure 8 shows the geometry used in the examples. Two representative spherical sampling schemes for $N = 14$ were used to arrange microphones and loudspeakers: maximum determinant grids [57] and icosahedral grids [58]. Use of maximum determinant grids significantly minimizes the effects of numerical integration at lower orders; however, middle and higher orders remain widely affected. In contrast, although the use of icosahedral grids does slightly affect the lower orders, their effects are more sparsely distributed along all orders. These facts are observed when contrasting Figs. 8b and 8c, where patterns $\Delta_{\nu\nu'\mu\mu'}^{(M)}\Delta_{\nu\nu''\mu\mu''}^{(L)}$ affecting reconstruction in (44) are shown for both grids. Icosahedral grids have been particularly used to distribute the microphones of the 252-channel recording system in [27], [28]. Although for simplicity the examples below use the same grid to arrange both microphones and loudspeakers, the effects of using distinct types of grids can be inferred because (35) clearly distinguishes the isolated and combined effects of sampling.

The overall effects of sampling are detailed in Fig. 9 by using the residual-to-signal ratios in (36). In general, the isolated effects of sampling $\mathcal{A}$ (see E_M), as well as the

coupled effects of sampling both $\mathcal{A}$ and $\mathcal{B}$ (see $E_{M,L}$), are more prominent than the isolated effects of sampling $\mathcal{B}$ (see E_L). Because maximum determinant grids ensure accurate integration on the spherical surfaces $\mathcal{A}$ and $\mathcal{B}$ at lower orders, they produce negligible residual-to-signal ratios at lower frequencies when using both $\mathcal{F}_\nu^{\text{ROlim}}$ and $\mathcal{F}_\nu^{\text{RFreg}}$. The benefits of using the proposed $\mathcal{F}_\nu^{\text{ROlim}}$ are more noticeable when using less uniform grids that do not ensure accurate integration, such as icosahedral ones, as can be observed in the smaller values of E_M and $E_{M,L}$ at lower and middle frequencies.

The local effects of band limitation and sampling with icosahedral grids when Ψ is reconstructed in a region of the horizontal plane are illustrated in Fig. 10 by using (25), (44), (45), (46), and (47). Contrasting the reconstruction results for $\mathcal{F}_\nu^{\text{RFreg}}$ (middle row) and $\mathcal{F}_\nu^{\text{ROlim}}$ (bottom row), it is observed that $\mathcal{F}_\nu^{\text{ROlim}}$ enables a greater reduction of ε_M and $\varepsilon_{M,L}$. As a consequence, $\mathcal{F}_\nu^{\text{ROlim}}$ produces smaller total reconstruction errors $\Psi - \Psi_{N;M,L}^{\text{disc}}$ in a wider area around the center.

Finally, the time-domain effects of band limitation and sampling are described in Fig. 11. Impulse responses were calculated by applying the inverse Fourier transform to the
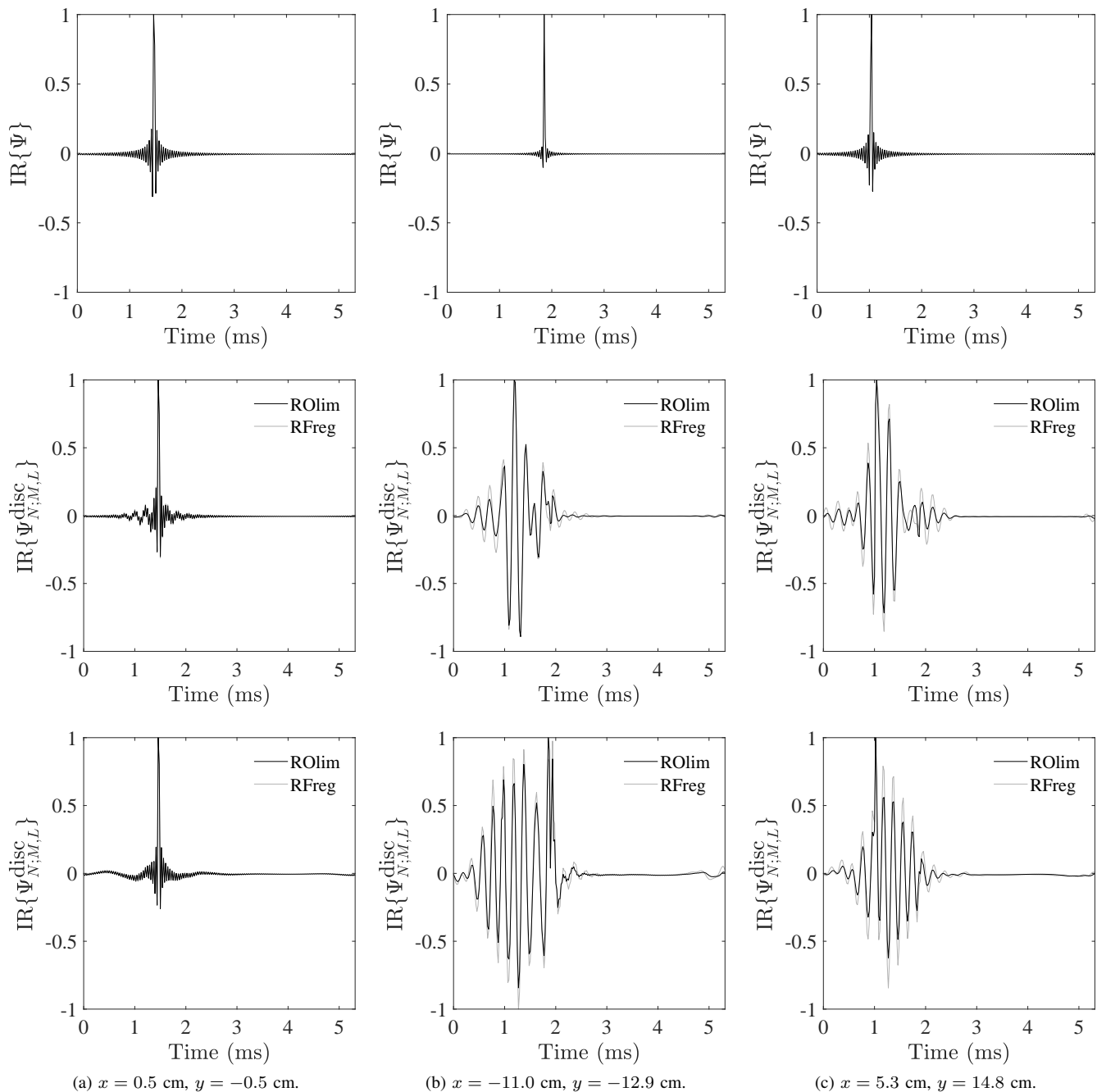
Fig. 11. Time-domain effects of sampling. Top panels show the normalized impulse responses (IRs) for the target signals Ψ, middle panels show the IRs reconstructed with maximum determinant grids, and bottom panels show the IRs reconstructed with icosahedral grids. Conditions are the same as those used in Figs. 9 and 10. Reconstructed IRs of $\Psi_{N;M,L}^{\mathrm{disc}}$ in (44) at three points $\vec{r}$ on the xy-plane are shown. Points near the microphone array's center are slightly affected by replication of main peaks, as shown in column (a). Points behind the array are more affected by backward replication, as shown incolumn (b). Points in front are more affected by forward replication, as shown in column (c). In general, the use of icosahedral grids produces more attenuated replications than use of maximum determinant grids. In both grids, $\mathcal{F}_{\nu}^{\mathrm{ROlim}}$ attenuates the replications even more when compared with $\mathcal{F}_{\nu}^{\mathrm{RFreg}}$, yielding IRs that are more localized around the main peaks.

discretization of $\Psi_{N;M,L}^{\mathrm{disc}}$ in frequency. Discretization was performed by using a sampling frequency of 48 kHz and a frame of 256 samples to ensure the visualization along the distances under consideration. By comparing the results for maximum determinant (middle panels) and icosahedral (bottom panels) grids, it can be generally observed that icosahedral grids yield impulse responses with more attenuated replications of main peaks. In both grids, by contrasting the impulse responses for

$\mathcal{F}_{\nu}^{\mathrm{ROlim}}$ (solid black line) and $\mathcal{F}_{\nu}^{\mathrm{RFreg}}$ (solid gray line), it can be further observed that the use of $\mathcal{F}_{\nu}^{\mathrm{ROlim}}$ enables a greater attenuation of replication effects, thereby yielding impulse responses that are more localized around the main peaks.

C. Comments on the perceptual aspects

Reconstruction of the sound pressure signals at the eardrums requires considering head-related transfer functions (HRTFs)

instead of the free-field transfer functions $\mathcal{T}^{\text{ff}}$ used in the above examples. Our objective evaluations therefore do not directly translate their performance to perceptual attributes, but we can nevertheless rely on recent numerical [29]–[32] and perceptual [24], [47], [49], [50] studies on binaural reconstruction from microphone array recordings and HRTFs to highlight the importance of using high-order representations when aiming toward the reconstruction of spatially accurate binaural signals.

In ideal recording and reproduction conditions with continuous spherical boundaries, high orders ensure the perception of more spatially sharp and more externalized sounds [24], [47]. High orders also reduce the distortions of perceived timbre caused by the rapid roll-off of SBMFs at higher frequencies (see Fig. 6) [49], [50].

In practice, however, the use of finite numbers of transducers produces two kinds of artifacts: low-frequency artifacts, perceived as ringing envelopes, and high-frequency artifacts, perceived as unpleasant sounds [24]. The development of high-resolution microphone arrays is crucial in this regard, as high-resolution HRTFs can be obtained with actual 3D model acquisition techniques and numerical acoustics methods.

The results for free-field conditions in Fig. 11 suggest that the proposed filters $\mathcal{F}_\nu^{\text{ROlim}}$ can help to reduce the perception of ringing sounds during binaural reconstruction because they have a smooth and bounded behavior at lower frequencies, and yield impulse responses that are highly concentrated around the main peaks. However, perceptual evaluations by means of detectability of differences, and localization tests along angles and distances, are necessary to provide more insight into the validity of the suggested approach.

VI. CONCLUSION

This paper has presented the theory of SBMFs for conversion of spherical microphone array signals into spherical loudspeaker array signals. SBMFs were obtained by examining the KHIE on the recording and reproduction boundaries and by further imposing a continuity condition. The particular case of a rigid recording boundary and an open reproduction boundary was addressed. As a result, new rigid-to-open SBMFs were formulated. A method for the design of smooth-and-bounded SBMFs for high-resolution arrays was also proposed as an alternative to existing ones. The method simply requires the specification of a gain threshold; it is equivalent to reducing the reconstruction radius at higher frequencies while the order truncation errors are kept bounded. The separate and combined effects of using finite numbers of microphones and loudspeakers were identified analytically and exemplified numerically. It was found that gain-limited rigid-to-open SBMFs can outperform existing filters based on Tikhonov regularization thanks to reduction of the combined sampling effects.

It is expected that the theory presented will contribute to the future formulation of SBMFs for non-concentric arrays as well as to the formulation of BMFs for other basic geometries and boundary conditions.

APPENDIX A
THE KIRCHHOFF–HELMHOLTZ INTEGRAL EQUATION

The Kirchhoff–Helmholtz integral equation (KHIE) is used to reconstruct a sound pressure field Φ at arbitrary observation point $\vec{r}$ within a source-free volume $\mathcal{V}$ from its values of pressure and normal derivative on the bounding surface $\mathcal{S}$ that delimits $\mathcal{V}$. The sound field is reconstructed at $\vec{r}$ by means of transfer functions $\mathcal{T}$ characterizing the transmission of sound from any point $\vec{r}_s$ on $\mathcal{S}$ to any point $\vec{r}$ in $\mathcal{V}$. The transfer function $\mathcal{T}$ is known as the Green's function. The KHIE reads [4]

$$
\begin{aligned}
\Phi(\vec{r}, k) = \int_{\vec{r}_s \in \mathcal{S}} \\
\left[\mathcal{T}(\vec{r}_s, \vec{r}, k) \frac{\partial}{\partial \vec{n}_s} \Phi(\vec{r}_s, k) - \Phi(\vec{r}_s, k) \frac{\partial}{\partial \vec{n}_s} \mathcal{T}(\vec{r}_s, \vec{r}, k) \right] d\vec{r}_s,
\end{aligned}
\tag{51}
$$

where $\vec{n}_s$ is the vector normal to $\mathcal{S}$ at $\vec{r}_s$, pointing outward $\mathcal{V}$, and $\frac{\partial}{\partial \vec{n}_s}$ denotes the derivative in the direction of $\vec{n}_s$.

APPENDIX B
SPHERICAL FOURIER TRANSFORMS

The angular solution to the Helmholtz equation defines the spherical harmonics $Y_\nu^\mu(\Omega)$ of order ν and degree μ [4],

$$
Y_\nu^\mu(\Omega) = \sqrt{\frac{2\nu + 1}{4\pi} \frac{(\nu - \mu)!}{(\nu + \mu)!}} P_\nu^\mu(\sin\phi) \exp(j\mu\theta), \tag{52}
$$

where P_ν^μ are the non-normalized associated Legendre functions. They are orthonormal on the unit sphere $\mathbb{S}^2$ [4],

$$
\int_{\Omega \in \mathbb{S}^2} Y_\nu^\mu(\Omega) \overline{Y_{\nu'}^{\mu'}(\Omega)} d\Omega = \delta_{\nu\nu'} \delta_{\mu\mu'}, \tag{53}
$$

where $d\Omega = \cos\phi\, d\phi\, d\theta$ and δ is the Kronecker delta. The angular part of a finite-energy acoustic pressure field Φ can be expanded in terms of spherical harmonics [4],

$$
\text{ISFT:} \quad \Phi(r, \Omega) = \sum_{\nu=0}^{\infty} \sum_{\mu=-\nu}^{\nu} \Phi_{\nu\mu}(r) Y_\nu^\mu(\Omega), \tag{54}
$$

where the expansion coefficients are defined by [4],

$$
\text{SFT:} \quad \Phi_{\nu\mu}(r) = \int_{\Omega \in \mathbb{S}^2} \Phi(r, \Omega) \overline{Y_\nu^\mu(\Omega)} d\Omega. \tag{55}
$$

In the mathematical literature [5], (55) is referred to as the spherical Fourier transform (SFT), and (54) is referred to as the inverse spherical Fourier transform (ISFT).

APPENDIX C
SBMFS BASED ON TIKHONOV REGULARIZATION

Transform-domain driving signals $\mathcal{D}_{\nu\mu}$ on $\mathcal{B}$ are obtained from recordings $\mathcal{P}$ on $\mathcal{A}$ by solving the linear system

$$
\mathcal{P}(\vec{a}_m, k) = \sum_{\nu,\mu}^{N} Y_\nu^\mu(\Omega_m) \mathcal{F}_\nu^{-1}(a, b, k) \mathcal{D}_{\nu\mu}(b, k) + \epsilon_m^{(N)}, \tag{56}
$$

where $m = 1, \cdots, M$. In matrix notation, (56) becomes

$$
\mathbf{P} = \left[\mathbf{Y} \mathbf{F}^{-1} \right] \mathbf{D} + \mathbf{E}, \tag{57}
$$

where $\mathbf{P} = \left[\mathcal{P}(\vec{a}_m)\right]_{M \times 1}$, $\mathbf{Y} = \left[Y_\nu^\mu(\Omega_m)\right]_{M \times (N+1)^2}$, $\mathbf{F}^{-1} = \mathrm{diag}\left(\mathcal{F}_\nu^{-1}\right)$, $\mathbf{D} = \left[\mathcal{D}_{\nu\mu}\right]_{(N+1)^2 \times 1}$, and $\mathbf{E} = \left[\epsilon_m^{(N)}\right]_{M \times 1}$.

A solution to (57) is found by Tikhonov regularization [56]:

$$\mathbf{D} = \min\left\{ \|\mathbf{YF}^{-1}\mathbf{D} - \mathbf{P}\|_2^2 + \|\lambda\mathbf{I}\|_2^2 \right\}$$
$$= \left(\left[\overline{\mathbf{F}^{-1}}^\top \underbrace{\overline{\mathbf{Y}}^\top \mathbf{Y}}_{\approx \mathbf{I}} \mathbf{F}^{-1} + \lambda^2\mathbf{I} \right]^{-1} \overline{\mathbf{F}^{-1}}^\top \right) \overline{\mathbf{Y}}^\top \mathbf{P}. \quad (58)$$

When assuming perfect quadrature on the sphere, the orthonormality residuals defined in (38) are neglected and the Gram matrix $\overline{\mathbf{Y}}^\top \mathbf{Y}$ in (58) results in an identity matrix of size $(N+1)^2$. The perfect quadrature assumption leads to

$$\mathbf{D} = \mathrm{diag}\left(\frac{\mathcal{F}_\nu}{1 + \lambda^2|\mathcal{F}_\nu|^2} \right) \overline{\mathbf{Y}}^\top \mathbf{P}, \quad (59)$$

the elements of whose resulting diagonal matrix define the regularized filters in (31).

REFERENCES

[1] F. M. Fazi and P. A. Nelson, "Nonuniqueness of the solution of the sound field reproduction problem with boundary pressure control," *Acta Acust. United Ac.*, vol. 98, no. 1, pp. 1–14, Jan. 2012.

[2] ——, "Sound field reproduction as an equivalent acoustical scattering problem," *J. Acoust. Soc. Am.*, vol. 134, no. 5, pp. 3721–3729, 2013.

[3] J. A. Hargreaves and Y. W. Lam, "An energy interpretation of the Kirchhoff-Helmholtz boundary integral equation and its application to sound field synthesis," *Acta Acust. United Ac.*, vol. 100, no. 5, pp. 912–920, Sep. 2014.

[4] E. G. Williams, *Fourier Acoustics: Sound Radiation and Nearfield Acoustical Holography*. London, UK: Academic Press, 1999.

[5] D. Healy, Jr., D. Rockmore, P. Kostelec, and S. Moore, "FFTs for the 2-sphere-Improvements and variations," *J. Fourier Anal. Appl.*, vol. 9, no. 4, pp. 341–385, Jul. 2003.

[6] G. H. Koopmann, L. Song, and J. B. Fahnline, "A method for computing acoustic fields based on the principle of wave superposition," *J. Acoust. Soc. Am.*, vol. 86, no. 6, pp. 2433–2438, 1989.

[7] S. Spors, R. Rabenstein, and J. Ahrens, "The theory of wave field synthesis revisited," in *Proc. 124th Convention Audio Eng. Soc.*, Amsterdam, The Netherlands, May 2008.

[8] J. Daniel, "Spatial sound encoding including near field effect: Introducing distance coding filters and a viable, new ambisonic format," in *23rd Int. Conf. Audio Eng. Soc.*, May 2003.

[9] S. Moreau, J. Daniel, and S. Bertet, "3d sound field recording with higher order ambisonics–Objective measurements and validation of a 4th order spherical microphone," in *Proc. 120th Convention Audio Eng. Soc.*, May 2006.

[10] J. Meyer and G. Elko, "A highly scalable spherical microphone array based on an orthonormal decomposition of the soundfield," in *Proc. IEEE ICASSP*, vol. II, Orlando, FL, USA, May 2002, pp. 1781–1784.

[11] B. Rafaely, "Analysis and design of spherical microphone arrays," *IEEE Trans. Speech, Audio Process.*, vol. 13, no. 1, pp. 135–143, Jan. 2005.

[12] B. Rafaely, B. Weiss, and E. Bachmat, "Spatial aliasing in spherical microphone arrays," *IEEE Trans. Signal Process.*, vol. 55, no. 3, pp. 1003–1010, Mar. 2007.

[13] Z. Li, R. Duraiswami, and N. A. Gumerov, "Capture and recreation of higher order 3d sound fields via reciprocity," in *Proc. Int. Conf. Auditory Display*, Sydney, Australia, Jul. 2004.

[14] Z. Li and R. Duraiswami, "Flexible and optimal design of spherical microphone arrays for beamforming," *IEEE Trans. Audio, Speech, Language Process.*, vol. 15, no. 2, pp. 702–714, Feb. 2007.

[15] D. N. Zotkin, R. Duraiswami, and N. A. Gumerov, "Plane-wave decomposition of acoustical scenes via spherical and cylindrical microphone arrays," *IEEE Trans. Aud. Speech & Lang. Proc.*, vol. 18, no. 1, pp. 2–6, Jan. 2010.

[16] E. Fisher and B. Rafaely, "Near-field spherical microphone array processing with radial filtering," *IEEE Trans. Audio, Speech, Language Process.*, vol. 19, no. 2, pp. 256–265, Feb. 2011.

[17] S. Yan, H. Sun, U. Svensson, X. Ma, and J. Hovem, "Optimal modal beamforming for spherical microphone arrays," *IEEE Trans. Audio, Speech, Language Process.*, vol. 19, no. 2, pp. 361–371, Feb. 2011.

[18] T. Rettberg and S. Spors, "Time-domain behaviour of spherical microphone arrays at high orders," in *Proc. DAGA*, 2014.

[19] S. Lösler and F. Zotter, "Comprehensive radial filter design for practical higher-order Ambisonic recording," in *Proc. DAGA*, 2015.

[20] D. Alon and B. Rafaely, "Beamforming with optimal aliasing cancellation in spherical microphone arrays," *IEEE/ACM Trans. Audio, Speech, Language Process.*, vol. 24, no. 1, pp. 196–210, Jan. 2016.

[21] J. Meyer and G. Elko, "A qualitative analysis of frequency dependencies in ambisonics decoding related to spherical microphone array recording," in *Proc. AES Int. Conf. Sound Field Control*. Guildford, UK: Audio Engineering Society, Jul. 2016.

[22] R. Duraiswami, D. N. Zotkin, Z. Li, E. Grassi, N. A. Gumerov, and L. S. Davis, "High order spatial audio capture and its binaural head-tracked playback over headphones with HRTF cues," in *AES 119*, New York, USA, Oct. 2005.

[23] W. Song, W. Ellermeier, and J. Hald, "Using beamforming and binaural synthesis for the psychoacoustical evaluation of target sources in noise," *J. Acoust. Soc. Am.*, vol. 123, no. 2, pp. 910–924, Feb. 2008.

[24] A. Avni, J. Ahrens, M. Geier, S. Spors, H. Wierstorf, and B. Rafaely, "Spatial perception of sound fields recorded by spherical microphone arrays with varying spatial resolution," *J. Acoust. Soc. Am.*, vol. 133, no. 5, pp. 2711–2721, May 2013.

[25] N. R. Shabtai and B. Rafaely, "Generalized spherical array beamforming for binaural speech reproduction," *IEEE/ACM Trans. Audio, Speech, Language Process.*, vol. 22, no. 1, pp. 238–247, Jan. 2014.

[26] N. R. Shabtai, "Optimization of the directivity in binaural sound reproduction beamforming," *J. Acoust. Soc. Am.*, vol. 138, no. 5, pp. 3118–3128, 2015.

[27] S. Sakamoto, S. Hongo, and Y. Suzuki, "3d sound-space sensing method based on numerous symmetrically arranged microphones," *IEICE Trans. Fundamentals*, vol. E97-A, no. 9, pp. 1893–1901, Sep. 2014.

[28] S. Sakamoto, S. Hongo, T. Okamoto, Y. Iwaya, and Y. Suzuki, "Sound-space recording and binaural presentation system based on a 252-channel microphone array," *Acoust. Sci. Technol.*, vol. 36, no. 6, pp. 516–526, 2015.

[29] C. D. Salvador, S. Sakamoto, J. Treviño, J. Li, Y. Yan, and Y. Suzuki, "Accuracy of head-related transfer functions synthesized with spherical microphone arrays," *Proc. Mtgs. Acoust.*, vol. 19, no. 1, Apr. 2013.

[30] C. D. Salvador, S. Sakamoto, J. Treviño, and Y. Suzuki, "Numerical evaluation of binaural synthesis from rigid spherical microphone array recordings," in *Proc. AES Int. Conf. Headphone Technology*. Aalborg, Denmark: Audio Engineering Society, Aug. 2016.

[31] ——, "Spatial accuracy of binaural synthesis from rigid spherical microphone array recordings," *Acoust. Sci. Technol.*, vol. 38, no. 1, pp. 23–30, Jan. 2017.

[32] ——, "Design theory for binaural synthesis: Combining microphone array recordings and head-related transfer function datasets," *Acoust. Sci. Technol.*, vol. 38, no. 2, pp. 51–62, Mar. 2017.

[33] M. Park and B. Rafaely, "Sound-field analysis by plane-wave decomposition using spherical microphone array," *J. Acoust. Soc. Am.*, vol. 118, no. 5, pp. 3094–3103, Nov. 2005.

[34] D. Khaykin and B. Rafaely, "Acoustic analysis by spherical microphone array processing of room impulse responses," *J. Acoust. Soc. Am.*, vol. 132, no. 1, pp. 261–270, 2012.

[35] H. Sun, E. Mabande, K. Kowalczyk, and W. Kellermann, "Localization of distinct reflections in rooms using spherical microphone array eigenbeam processing," *J. Acoust. Soc. Am.*, vol. 131, no. 4, pp. 2828–2840, 2012.

[36] S. Tervo and A. Politis, "Direction of arrival estimation of reflections from room impulse responses using a spherical microphone array," *IEEE/ACM Trans. Audio, Speech, Language Process.*, vol. 23, no. 10, pp. 1539–1551, Oct. 2015.

[37] D. A. Russell, "Basketballs as spherical acoustic cavities," *Am. J. Phys.*, vol. 78, no. 6, pp. 549–554, 2010.

[38] D. B. Ward and T. Abhayapala, "Reproduction of a plane-wave sound field using an array of loudspeakers," *Speech and Audio Processing, IEEE Transactions on*, vol. 9, no. 6, pp. 697–707, Sep. 2001.

[39] J. Ahrens and S. Spors, "An analytical approach to sound field reproduction using circular and spherical loudspeaker distributions," *Acta Acust. United Ac.*, vol. 94, no. 6, pp. 988–999, Nov. 2008.

[40] ——, "A modal analysis of spatial discretization of spherical loudspeaker distributions used for sound field synthesis," *IEEE Trans. Audio, Speech, Language Process.*, vol. 20, no. 9, pp. 2564–2574, Nov. 2012.

[41] Y. J. Wu and T. D. Abhayapala, "Theory and design of soundfield reproduction using continuous loudspeaker concept," *IEEE Trans. Audio, Speech, Language Process.*, vol. 17, no. 1, pp. 107–116, Jan. 2009.

[42] M. A. Poletti, "Three-dimensional surround sound systems based on spherical harmonics," *J. Audio Eng. Soc.*, vol. 53, no. 11, pp. 1004–1025, 2005.

[43] F. Zotter, "Analysis and Synthesis of Sound-Radiation with Spherical Arrays," Doctoral Thesis, Universitat fur Musik und Darstellende Kunst, Graz, Austria, Sep. 2009.

[44] H. Morgenstern, B. Rafaely, and F. Zotter, "Theory and investigation of acoustic multiple-input multiple-output systems based on spherical arrays in a room," *J. Acoust. Soc. Am.*, vol. 138, no. 5, pp. 2998–3009, 2015.

[45] H. Morgenstern, B. Rafaely, and M. Noisternig, "Design framework for spherical microphone and loudspeaker arrays in a multiple-input multiple-output system," *J. Acoust. Soc. Am.*, vol. 141, no. 3, pp. 2024–2038, 2017.

[46] N. A. Gumerov and R. Duraiswami, *Fast multipole methods for the Helmholtz equation in three dimensions*, ser. Elsevier Series in Electromagnetism.   Maryland, USA: Elsevier, 2004.

[47] B. Bernschütz, A. V. Giner, C. Pörschmann, and J. Arend, "Binaural reproduction of plane waves with reduced modal order," *Acta Acust. United Ac.*, vol. 100, no. 5, pp. 972–983, Sep. 2014.

[48] C. D. Salvador, S. Sakamoto, J. Treviño, and Y. Suzuki, "Distance-varying filters to synthesize head-related transfer functions in the horizontal plane from circular boundary values," *Acoust. Sci. Technol.*, vol. 38, no. 1, pp. 1–13, Jan. 2017.

[49] J. Sheaffer, S. Villeval, and B. Rafaely, "Rendering binaural room impulse responses from spherical microphone array recordings using timbre correction," in *Proc. of the EAA Joint Symp. Auralization and Ambisonics*, Berlin, Germany, Mar. 2014.

[50] Z. Ben-Hur, F. Brinkmann, J. Sheaffer, S. Weinzierl, and B. Rafaely, "Spectral equalization in binaural signals represented by order-truncated spherical harmonics," *J. Acoust. Soc. Am.*, vol. 141, no. 6, pp. 4087–4096, 2017.

[51] L. G. Copley, "Fundamental results concerning integral representations in acoustic radiation," *J. Acoust. Soc. Am.*, vol. 44, no. 1, pp. 28–32, 1968.

[52] P. A. Nelson and Y. Kahana, "Spherical harmonics, singular-value decomposition and the head-related transfer function," *J. Sound Vib.*, vol. 239, no. 4, pp. 607 – 637, 2001.

[53] H. Sun, S. Yan, and U. P. Svensson, "Optimal higher order ambisonics encoding with predefined constraints," *IEEE Trans. Aud. Speech & Lang. Proc.*, vol. 20, no. 3, pp. 742–754, Mar. 2012.

[54] D. A. Russell, J. P. Titlow, and Y.-J. Bemmen, "Acoustic monopoles, dipoles, and quadrupoles: An experiment revisited," *Am. J. Phys.*, vol. 67, no. 8, pp. 660–664, 1999.

[55] R. O. Duda and W. L. Martens, "Range dependence of the response of a spherical head model," *J. Acoust. Soc. Am.*, vol. 104, no. 5, pp. 3048–3058, Nov. 1998.

[56] A. Neumaier, "Solving ill-conditioned and singular linear systems: A tutorial on regularization," *SIAM Review*, vol. 40, no. 3, pp. 636–666, 1998.

[57] R. S. Womersley and I. H. Sloan, "How good can polynomial interpolation on the sphere be?" *Adv. Comput. Math.*, vol. 14, pp. 195–226, Apr. 2001.

[58] R. Sadourny, A. Arakawa, and Y. Mintz, "Integration of the nondivergent barotropic vorticity equation with an icosahedral-hexagonal grid for the sphere 1," *Mon. Wea. Rev.*, vol. 96, no. 6, pp. 351–356, Jun. 1968.

César D. Salvador graduated from the Pontifical Catholic University of Peru in 2005. He received his M.Sc. degree in 2013 and his Ph.D. degree in 2016, both from the Graduate School of Information Sciences of Tohoku University. He is currently an Assistant Professor at the Research Institute of Electrical Communication of Tohoku University. His research interests include theoretical acoustics, spatial hearing, array signal processing, and high-definition 3D audio technology.

Shuichi Sakamoto received his B.S., M.Sc., and Ph.D. degrees from Tohoku University, in 1995, 1997, and 2004, respectively. He is currently an Associate Professor at the Research Institute of Electrical Communication, Tohoku University. He was a Visiting Researcher at McGill University, Montreal, Canada during 2007-2008. His research interests include human multi-sensory information processing including hearing, speech perception, and the development of high-definition 3D audio recording systems. He is a Member of ASJ, IEICE, VRSJ, and other professional societies.

Jorge Treviño graduated from the Monterrey Institute of Technology and Higher Education in 2005. He received the degree of M.Sc. in 2011 and a Ph.D. in information sciences in 2014, both from the Graduate School of Information Sciences of Tohoku University. He is currently an Assistant Professor in the Research Institute of Electrical Communication of Tohoku University. His research interests include sound field recording and reproduction, array signal processing, and spatial audio.

Yôiti Suzuki graduated from Tohoku University in 1976 and received his Ph.D. degree in electrical and communication engineering in 1981. He is currently a Professor at the Research Institute of Electrical Communication, Tohoku University. His research interests include psychoacoustics, multimodal perception, high-definition 3D auditory displays, and digital signal processing of acoustic signals. He has received the Awaya Kiyoshi Award and Sato Prize from the Acoustical Society of Japan, as well as the FIT Funai Best Paper Award.